國立交通大學

材料科學與工程學研究所

碩 士 論 文

多孔性二氧化矽於新穎低介電底部填膠材料之封孔研究

Pore Sealing Studies of Porous Silica for Novel Low-K Underfill Materials

研 究 生：陳冠宇

指導教授：呂志鵬 教授

中 華 民 國 九十六 年 十二 月

多孔性二氧化矽於新穎低介電底部填膠材料之封孔研究

Pore Sealing Studies of Porous Silica for Novel Low-K Underfill Materials

研 究 生：陳冠宇　　　　Student：Guan-Yu Chen
指導教授：呂志鵬　　　　Advisor：Dr. Jihperng (Jim) Leu

國 立 交 通 大 學
材 料 科 學 與 工 程 學 系
碩 士 論 文

A Thesis
Submitted to Department of Materials Science and Engineering
College of Engineering
National Chiao Tung University
in partial Fulfillment of the Requirements
for the Degree of
Master
in

Materials Science and Engineering

December 2007

Hsinchu, Taiwan, Republic of China

中華民國九十六年十二月

多孔性二氧化矽於新穎低介電底部填膠材料之封孔研究

學生: 陳冠宇 指導教授:呂志鵬 教授

國立交通大學材料與工程學系碩士班

摘要

底部填膠(underfill)材料已經廣泛的應用在覆晶封裝中，其作用為填滿晶片與基板間的間隙以避免凸塊(solder bumps)失效的產生，然而在射頻元件的應用中，底部填膠材料除了要有良好的熱機械性質，也要具備低介電常數以降低在高使用頻率下能量的耗損。本研究利用多孔性二氧化矽填充物的孔洞(介電常數為1)發展出具備低介電常數的底部填膠材料。吾人使用一種無機的材料(hexamethylcyclotrisiloxane,D3)先在低溫下封住多孔性二氧化碳的孔洞，然後在底部填膠的膠聯反應過程中加熱移除。首先,吾人利用示差掃描熱量計(DSC)和流變儀(Rheometer)去探討硬烤(curing)和粘度的行為，然後設計出封孔預處理所需的溫度流程，在95℃下，D3可以封住部分通孔，甚至全部的通孔，在3:1的D3對多孔性二氧化矽重量分率封孔處理後，孔洞體積和表面積降低了約50%。然後，在膠聯反應過程中，D3於125℃ ~165℃汽化由孔洞跑出，阻礙環氧樹脂灌入孔洞，因而成功的留下孔洞，此外，吾人利用氮氣吸脫附儀(BET)和掃瞄式電子顯微鏡(SEM)去研究探討D3和環氧樹脂(epoxy resins)之間的表面形貌與封孔機制。吾人成功的利用封孔材料對 15 wt%孔洞性的二氧化矽填充物進行封孔預處理，將介電常數由 3.2 降低至 2.86(10.6%)。然而，由於(1)多孔性二氧化矽的孔洞結構,(2)和硬烤過程中，D3 汽化而破壞環氧樹脂和二氧化矽間的界面接著，最後使得底部填膠的機械性質由 3 GPa 降低至 1.5GPa。

Pore Sealing Studies of Porous Silica for Novel Low-K Underfill Materials

Student: Guan-Yu Chen Advisors: Dr. Jihperng (Jim) Leu

Department of Material Science and Engineering

National Chiao Tung University

Abstract

Underfill materials had been widely employed in the flip-chip packaging to fill the gap of solder bumps connecting IC chip and organic substrate in order to prevent failure of the solder joints. For radio-frequency (RF) device applications, underfill materials shall possess low dielectric constant to alleviate power loss at high-frequency, in addition to good thermal and mechanical properties. In the thesis, a novel approach by incorporating porosity through porous silica filler was attempted to develop low-k underfill materials. An inorganic, sacrificial material, hexamethylcyclotrisiloxane (D3), was employed to temporarily seal the interconnected pores in the porous silica at low temperature, and was later removed thermally during the crosslinking reaction. The viscosity and curing behavior of epoxy resins was first investigated by differential scanning calorimetry (DSC) and rheometer to design temperature profile for pore-sealing pretreatment and outgassing of sacrificial material. We found that D3 either completely or partially sealed the connected pores at 95 ℃ with volume and surface area reduction up to ~50% at the 3:1 weight ratio of D3 to porous silica. D3 outgassed during crosslinking reaction (125 ~ 165 ℃), and successfully leaved porosity within the interconnect pores

without the back-flow of epoxy resins. In addition, the morphology of D3/porous silica and pore sealing mechanism were studied by scanning electronic microscopy (SEM) and Brunauer-Emmett-Teller method (BET). We successfully developed a pore-sealing pretreatment of porous silica filler by a sacrificial material to reduce dielectric constant from 3.2 to 2.86 or 10.6% with 15% filler. However, resulting from that (1) porous silica possessed porous structure, and (2) D3 vaporized and diffused out of pores during curing reaction, which destroyed the adhesion between epoxy resins and silica fillers, the mechanical strength was also reduced from 3.0 GPa to 1.5 GPa.

誌謝

有一句話叫做活到老學到老，人的一生本來就是不斷地學習，並充實自己。很高興我的碩士的學習生涯，終於告一段落，兩年多的時間在一生中雖不算長，但是 NIP 實驗室就像漫畫裡的精神時光屋，讓我的每天都過的相當充實，也讓我從大學畢業的毛頭小子，蛻變成一個可以為社會貢獻一分小小心力的研究生，未來的日子裡，我依然會繼續學習成長，但現在我只想要感謝那些在我身邊，給予我幫助及鼓勵的人們。

首先我要感謝 NIP 的大家長呂志鵬老師，能進這實驗室真是我的福氣，呂老師是我這一生到現在碰過最好的一位老師，因為老師的教學熱誠，厚植了我對材料工程領域之基礎學科知識，以及跨其他領域之學習能力；因為老師的平易近人，培養了我在團隊合作中、溝通、整合及領導之能力；因為老師的以身作則，健全了我人格之養成，並且了解學習關懷社會並珍惜地球環境資源的重要性。呂志鵬老師實在是我的良師，更是我的益友，讓我這段精神時光屋之旅，過得一百分的充實。

另外，感謝國科會(計畫編號:NSC95-2221-E009-309/NSCXXXXX)與SRC/UMC(計畫編號:SRC-1301.001)於實驗經費的贊助，以及工研院康宏洲和信越矽利光公司洪西宗先生等人在技術和資源上的大力協助。接下來，我要謝謝實驗室的學長們：國原、元辰、牧龍、子豪、昱涵、志安等，謝謝你們在實驗以及生活上的幫助及教導。還有我要謝謝學弟學妹們，怡臻、少農、欣源、王智、詩雅等等，雖然你們沒幫上忙，還是謝謝你們。最後我要感謝我的同窗好友季高跟鈞元，尤其是鈞元，陪我戰至一兵一卒，走到最後一天一起出精神時光屋，謝謝。

最後的最後，我要謝謝一值在我身邊給我鼓勵及安慰的女友小蘋，謝謝妳溫暖的陪伴。我還要謝謝我的家人，謝謝你們在精神及經濟上的無條件支持，我願意把所有的榮耀獻給我最愛的你們，謝謝^^。

Contents

摘要 I
Abstract II
誌謝 IV
Contents V
List of Tables VII
List of Figures VIII
Chapter 1 Introduction 1
Chapter 2 Literature Review and Motivations 3
2.1 Electronic Packaging 3
2.2 Flip-Chip Packaging 7
2.3 Underfill materials 12
2.3.1 Introduction of Underfill Materials 12
2.3.2 Underfill materials and Low-K Flip Chip Packaging 16
2.3.3 Underfill Materials and RF Electronic Packaging 20
2.3.3.1 RF Devices and Flip Chip Packaging 20
2.3.3.2 Underfill Materials for RF Devices 20
2.4 Motivation of Thesis 22
Chapter 3 Experimental 26
3.1 Sample Preparation 26
3.1.1 Chemicals 26
3.1.1.1 Pore-Sealing Pretreatment 27
3.1.2 Preparation of underfill materials 29
3.1.2.1 Curing Profiles of Underfill materials 31
3.2 Experimental Approaches 34
3.3 Instrumentation 36
3.3.1 Differential Scanning Calorimetry (DSC) 36
3.3.2 Rheometer [40] 38
3.3.3 Brunauer-Emmett-Teller gas adsorption method (BET) 40
3.3.4 RF Impedance-Material Analyzer 43
3.3.5 Dynamic Mechanical Analyzer (DMA) 45
3.3.5.1 Fundamental Theory 45
3.3.5.2 Characterization of Adhesion 46
Chapter 4 Results and Discussion 48
4.1 Selection of pre-sealing materials by thermal reactivity and viscosity 48
4.2 Characterization of Pore-Sealing Treatment 51
4.2.1 Pore-Sealing Treatment by N-Butanol 51

4.2.2 Pore-Sealing Treatment by Hexamethylcyclotrisiloxane (D3)...........55
4.2.2.1 Morphology of D3 materials and porous silica fillers 56
4.2.2.2 Brunauer-Emmett-Teller Method (BET) 59
4.3 Dielectric constants of low-k underfill materials..67
4.4 Moduli of low-k underfill materials..70
Chapter 5 Conclusions 77
References...80

List of Tables

Table 2.1 Comparison among wire bond, TAB, and FC 7
Table 2.2 Four common types of underfill materials 12
Table 2.3 Common epoxy resins 13
Table 2.4 Properties of dielectric materials 17
Table 2.5 Electronic polarizability 22
Table 3.1 Formulation of the conventional capillary underfill material 29
Table 3.2 Formulations of low-k underfill materials A and B, without pore-sealing pretreatment 30
Table 3.3 Formulations of the low-k underfill materials C, D, and E, with pore-sealing pretreatment 30
Table 4.1 Formulation underfill material A 53
Table 4.2 BET data of porous silica in low-k underfill materials B, C, and D 62
Table 4.3 Dielectric constants of various underfill materials 67
Table 4.4 Moduli of various underfill materials 70
Table 4.5 Loss factor, tan δ of low-k underfill materials B, C, and D 73

List of Figures

Figure 2.1 Five different levels of electronic packaging 4
Figure 2.2 cross-sectional view and top view of Ball Grid Array (BGA) 5
Figure 2.3 Directions of electronic packaging....................6
Figure 2.4 Structure of a flip chip....................8
Figure 2.5 Bumping process 9
Figure 2.6 Bumps alignment and reflow....................10
Figure 2.7 Self-alignment of solder bumps....................10
Figure 2.8 Underfill dispensing process 11
Figure 2.9 Structure of epoxy resins....................12
Figure 2.10 Curing mechanism of epoxy resins 13
Figure 2.11 Common (a) hardeners and (b) catalysts in underfill materials [21]....14
Figure 2.12 Hydrolysis reaction: $Si(OH)_4 + H_2O$ 15
Figure 2.13 Polymerization reaction....................15
Figure 2.14 General structure of low-k flip chip package 17
Figure 2.15 Crack and delamination of low-k layer 18
Figure 2.16 Bump cracking....................19
Figure 2.17 Directions of underfill materials development [30] 19
Figure 2.18 Two epoxy resins: (a) bisphenol-A type epoxy resins (b)fluorinated epoxy resins 23
Figure 2.19 Incorporation of porosity into low-k layer 24
Figure 3.1 Chemical structures of (a) Epikote^{TM} 828 (b) Epikote^{TM} 862 (c)MEHHPA (d) 2E4MI....................27
Figure 3.3 DSC curves of (a) low-k underfill material A and (2) low-k underfill material B....................33
Figure 3.4 Flow-chart of experimental procedures....................35
Figure 3.5 Heat Flux DSC 36
Figure 3.6 Power Compensation DSC....................37
Figure 3.7 Typical DSC curves of some general polymer transitions 37
Figure 3.8 Structure of rheometer....................38
Figure 3.9 Typical BET curves : (a) non-pores (b) macropores (c) mesopores (d) micropores....................42
Figure 3.10 RF Impedance/Material Analyzer....................44
Figure 3.11 The response of materials in DMA 45
Figure 4.1 DSC curve of low-k underfill material B without pretreatment..............49
Figure 4.2 Viscosity as a function of temperature for low-k underfill material B....49

Figure 4.4 Three issues of cured low-k underfill material E: (a) bad mechanical strength, (b) bubbles on the surface and (c) phase separation 51
Figure 4.5 DSC curve of low-k underfill material E 53
Figure 4.6 DSC curve of Formulation underfill material A.....................................54
Figure 4.7 DSC curve of Low-k underfill materials with pore-sealing pretreatment by D3..56
Figure 4.8 Morphology of (a) hexamethylcyclotrisiloxane (D3) and (b) porous silica by SEM 57
Figure 4.9 Morphology of porous silica after pore-sealing treatment in (a) low-k underfill material C and (b) Low-k underfill material D by SEM...........58
Figure 4.10 BET curve of low-k underfill material B...60
Figure 4.11 BET curve of low-k underfill material C...60
Figure 4.12 BET curve of low-k underfill material D 61
Figure 4.13 Pore size distribution of porous silica in low-k underfill material B, without pore-sealing pretreatment 63
Figure 4.14 Pore size distribution of porous silica in low-k underfill material C, with pore-sealing pretreatment at 1 : 1 weight ratio 63
Figure 4.15 Pore size distribution of porous silica in low-k underfill material D, with pore-sealing pretreatment at 1 : 3 weight ratio 64
Figure 4.16 Comparison of these pore size distributions of porous silica with three different pretreatments 64
Figure 4.17 2-D pore-sealing model..66
Figure 4.18 Structure of zeeospheres..69
Figure 4.19 Moduli of calculated values and experimental data of low-k underfill materials B, C, and D 72
Figure 4.20 Morphology of cured underfill materials without pore-sealing pretreatment (low-k underfill material B) by SEM...............................74
Figure 4.21 Morphology of cured underfill materials with the pore-sealing pretreatment (low-k underfill materials C and D) by SEM 76

Chapter 1 Introduction

Silicon-based integrated circuit (IC) devices continued scaling toward 45 nm node [1], while the products became smaller and faster with more functionalities and complexity [2]. Flip-chip technology, which utilized an area array of solder bumps to connect IC chip and organic or ceramic substrate, has been widely adopted in the packaging of microprocessors, graphic chips, and DSP chips due to its advantages such as high I/O density and short interconnects [3]. In the reliability of flip-chip packaging, the most challenging problem was the solder joint fatigue which mainly arose from thermal mechanical stress induced during temperature cycle due to coefficient of thermal expansion (CTE) mismatch between silicon chip and substrate. The solder joints reliability could be solved by using underfill materials, which consisted of epoxy resins, hardner, catalyst and silica fillers, and offered mechanical properties ranging from rigid to compliant depending on the requirements dictated by the solder type and the low-k dielectrics in the copper interconnect [4-6].

In addition to the thermo-mechanical properties, the electric properties, especially the dielectric constant of underfill materials played an important role in power dissipation [7] in the flip-chip packaging. Higher operating frequency would cause an increase of power consumption if dielectric constant is fixed. With the explosive growth in cell phones and wireless products, radio-frequency (RF) devices (up to 100 GHz) have become the mainstream products in microelectronics industry. Such RF devices might suffer large loss of RF energy when operated at high-frequency [8, 9]. As a result, underfill materials shall possess low dielectric constants to alleviate power loss and excellent mechanical properties to support solder joints to ensure solder joints reliability for high-frequency applications.

In this thesis, we focused on developing low dielectric constant (low-k) underfill materials by incorporating porosity (k_{vacuum} = 1) through zeeospheres and porous silica fillers. For porous silica-based underfill materials, an inorganic sacrificial material, hexamethylcyclotrisiloxane (D3), was employed to temporarily seal the interconnected pores in the porous silica at temperature < 95 ℃, then removed thermally around 120 ~ 140℃ during the crosslinking reaction of epoxy materials. The pore-sealing pretreatment and curing profile were first investigated by differential scanning calorimetry (DSC) and rheometer. Then the morphology of D3/porous silica, pore-sealing mechanism were studied and proposed based on scanning electronic microscopy (SEM) and Brunauer-Emmett-Teller method (BET) techniques. Finally, the dielectric constants and moduli of underfill materials with different types of fillers were examined and discussed. Besides, these two properties of underfill materials, with or without pore-sealing pretreatment were also studied.

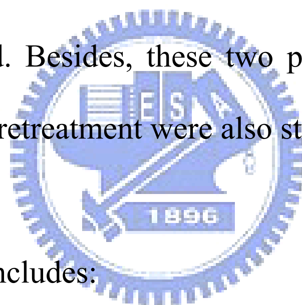

The organization of thesis includes:

(1) Chapter 1 Introduction

(2) Chapter 2 Literature review and Motivations

(3) Chapter 3 Experimental

(4) Chapter 4 Results and Discussion

(5) Chapter 5 Conclusions

Chapter 2 Literature Review and Motivations

2.1 Electronic Packaging

The process of electronic products typically involves wafer growth, circuit design, chip manufactures, packaging, and testing. Electronic packaging is one of the key technologies in the backend interconnects. The main functions of the electronic packaging [10-11] are:

(1) to support and protect IC devices

(2) to supply the power to IC devices

(3) to transmit the signals

(4) to dissipate the heat

The electronic packaging can be divided into five different levels in Figure 2.1 [3].

(1) The zero level packaging:

It involves the circuit design and fabrication of IC chips.

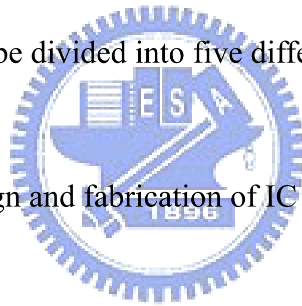

(2) The first level packaging:

This 1st level packaging sticks these chips into a packaging box. In addition, it also completes the circuit interconnection and seals the chips. This 1st level packaging is also called the chip-level packaging.

(3) The second level packaging:

In this packaging, the devices, completed in the first level packaging, connect to the printed circuit boards.

(4) The third level packaging:

This packaging connects several printed circuit boards to a motherboard.

(5) The forth level packaging:

In this level of packaging, different motherboards are combined to form an electronic product.

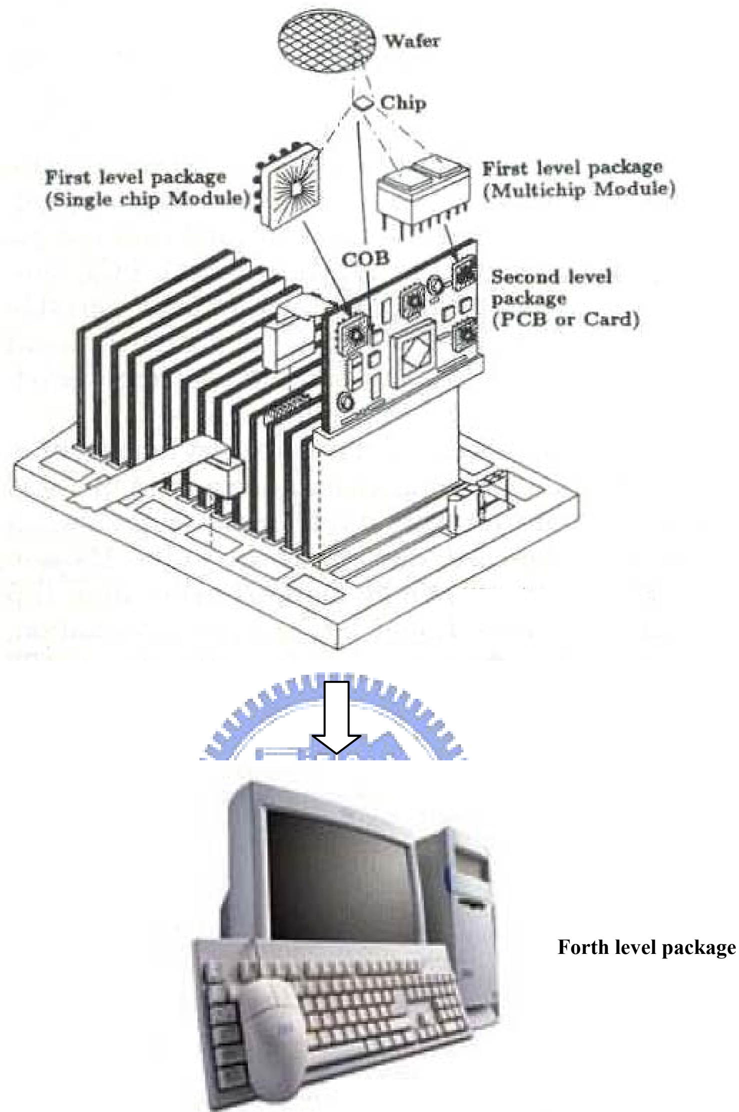

Figure 2.1 Five different levels of electronic packaging [3]

With the development toward lighter and smaller electronic products, the electronic packaging technologies are also improved steadily. Figure 2.3 shows the directions for the development of electronic packaging in terms of pin counts and size. Specifically, there are three phases below [13]:

(1) The first phase [13]:

The main change in this phase is the packaging type, which is developed from pin through holes (PTH) to surface mount technology (SMT). Many packaging technologies originate with the occurrence of surface mount technology. All of the electronic packaging trend toward higher I/O density and smaller pitch.

(2) The second phase [13]:

The main change in this phase is the arrangement of the pins. The arrangement is transformed from dual line and quadrangle arrangement into area one. Therefore, ball grid array (BGA) was invented to offer higher I/O numbers as shown in Figure 2.2.

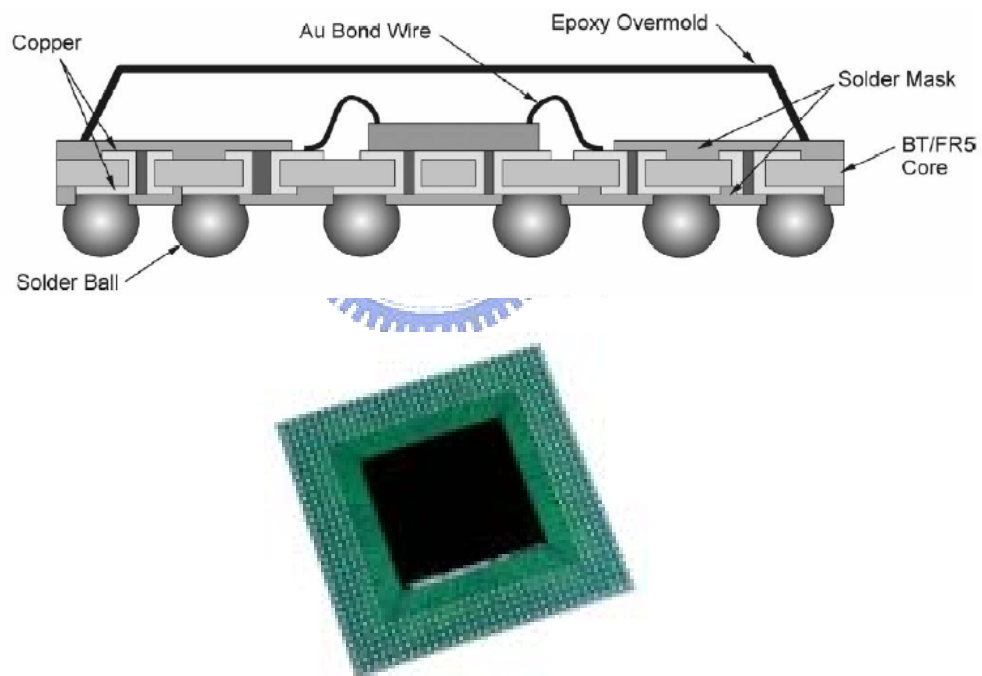

Figure 2.2 cross-sectional view and top view of Ball Grid Array (BGA) [12, 13]

(3) The third phase [13]:

Trending towards more I/O numbers and devices, the size of packaging boxes becomes larger; however, it results in reliability problem. The solution is to narrow the plastic part of packaging box; namely, the volume of packaging box is

equal to the chip. A technology, so-called chip scale package (CSP), was developed.

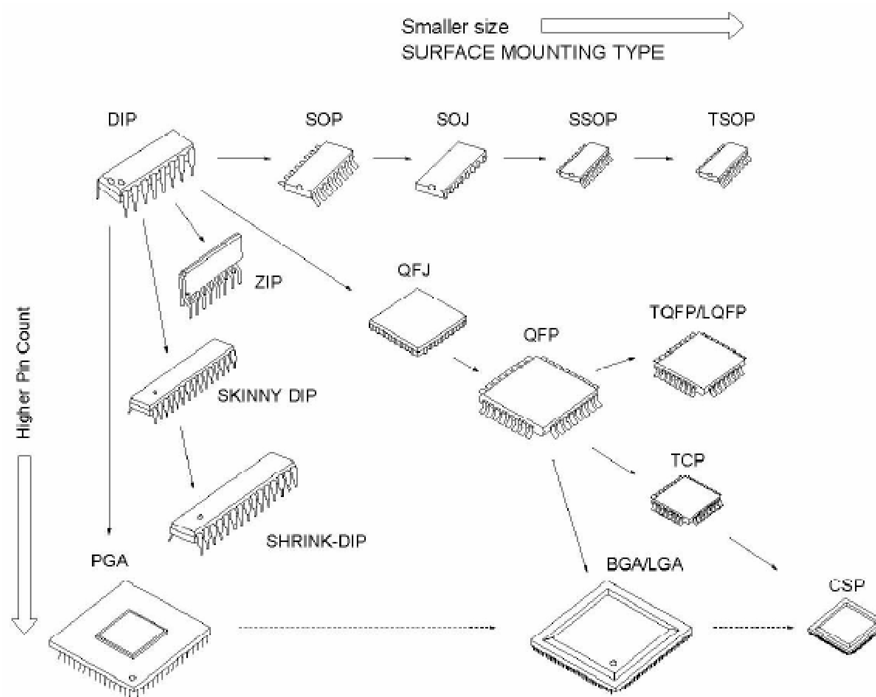

Figure 2.3 Directions of electronic packaging development [13]

Regarding the development of electronic packaging, the flip chip (FC) technology has been developed to skip the first level packaging and combine chips with printed circuit board directly.

2.2 Flip-Chip Packaging [3]

There are three methods to connect chips and printed circuit boards; i.e. (1) wire bonding (2) tap automated bonding (TAB) (3) flip chip (FC). With the steady increase of I/O numbers, the adoption of flip chip rises up gradually in the industry. Table 2.1 lists the comparison among these three methods.

Flip chip packaging technology is also called C4 (controlled-collapse chip connection) which was invented by IBM in 1960 [3]. The general structure of flip chip is shown in Figure 2.4. The main advantages of flip chip packaging below include:

Table 2.1 Comparison among wire bond, TAB, and FC [14, 15]

	Wire bond	TAB	Flip chip
Area ratio	1	1.33	0.33
Weight ratio	1	0.25	0.2
Thickness ratio	1	0.67	0.52
I/O numbers	300~500	500~700	>1000
Bond pad pitch	~50 μm	40 μm	~150 μm
Ball size	~40 μm	NA	~150 μm
Interval of bond pad	100~180 μm	80 μm	~300 μm

(1) Higher efficiency of space:

Chips are attached to the substrate directly; thus the process spares much space so that the height and area of the package are reduced [3].

(2) Higher I/O numbers:

Flip chip technology utilizes the bottom part of chips to carry out the input and output which results in more area to set up I/O pins. In addition, the I/O pins

become shorter connection path due to the wireless.

(3) Better heat dissipation and performance:

High I/O numbers and short interconnect dissipate heat more easily and enhance the performance.

(4) Improved reliability:

The connection of flip chip improve the reliability of devices by solder bumps instead of wires

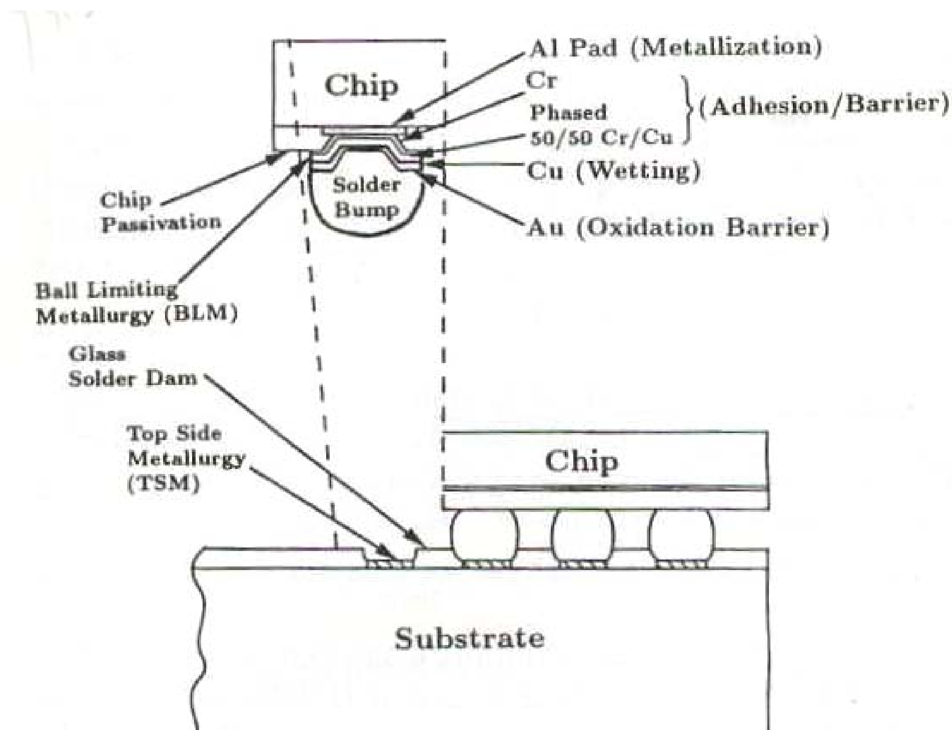

Figure 2.4 Structure of a flip chip packaging [3]

Flip chip technology utilizes evaporation, stencil printing, and electroplating methods to produce solder bumps on the metal pads of chips first. Second, chips are reversed to connect the substrate by the reflow of solder bumps. There are three main processes in the flip chip packaging described in details as follows [13, 16]:

(1) Flip Chip Bumping:

Recently, typical bumps are eutectic bump (63Sn/37Pb bump) and high lead bump (5Sn/95Pb bump). Figure 2.5 illustrates the bumping process. In this flip chip bumping process, the under bump metallurgy layer (UBM) is grown onto the bumps first. UBM mainly consists of three metal layers [17]:

a. Adhesion Layer:

The layer is employed to enhance the adhesion of bumps to metal pads and passivation layers. The materials are Ti and Cr.

b. Diffusion Barrier Layer:

The purpose of this layer is to prevent from the occurrence of intermetallic compounds arising from the reaction between bumps and metal pads. The chief materials are Cu and Ni.

c. Wetting Layer:

The function of this layer is to increase the adhesion between bumps and adhesion layers. The materials are Au and Ag.

Due to the concerns and regulations on the environmental contamination by lead, lead-free bump is being adopted gradually.

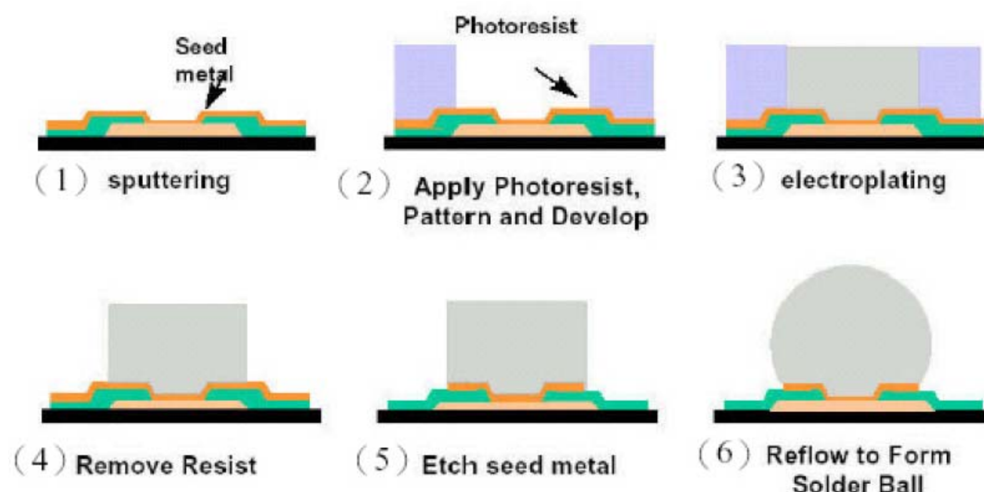

Figure 2.5 Bumping process [3, 18]

(2) Flip Chip Bonding [19]:

In this step, the bumps are coated with flux and aligned first, and then chips connect with substrate by reflow process as shown in Figure 2.6. During the reflow process, bumps have excellent self-alignment ability [20] as shown in Figure 2.7.

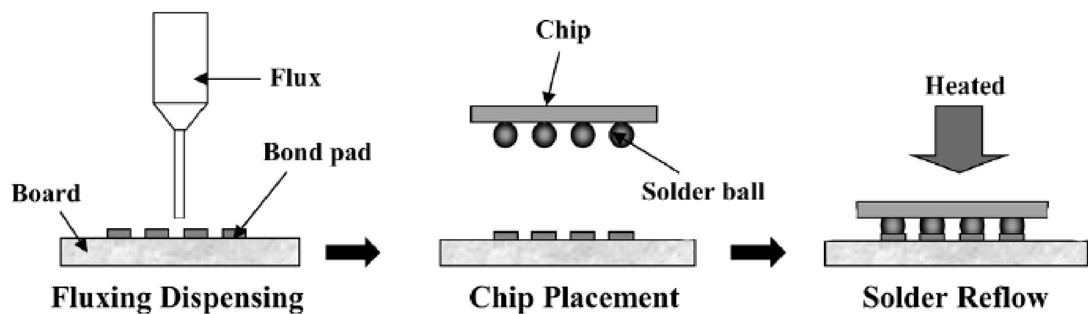

ES A 1896

Figure 2.6 Bumps alignment and reflow

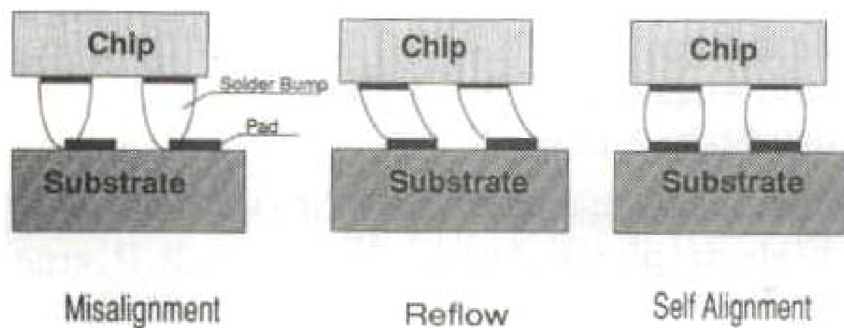

Figure 2.7 Self-alignment of solder bumps

(3) Underfill Dispensing [13, 19]:

In this process, the residual flux is cleaned first, and then underfill materials are dispensed to the gap between chip and substrate fully by capillarity. Finally, the underfill materials cure to protect the solder bumps. Figure 2.8 shows the under-dispensing process.

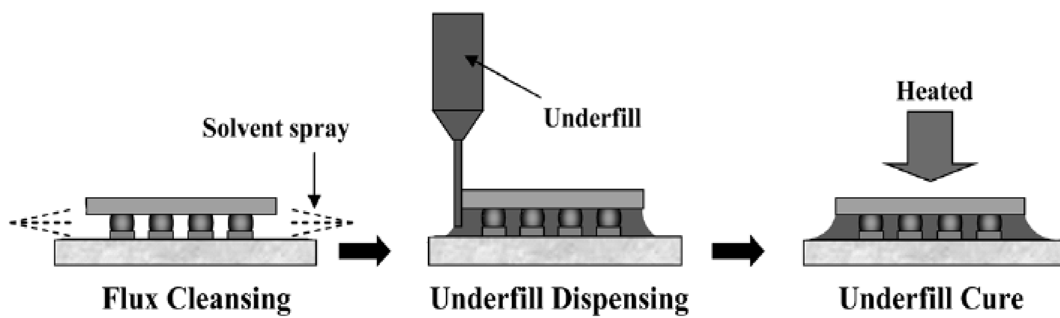

Figure 2.8 Underfill dispensing process

2.3 Underfill materials

2.3.1 Introduction of Underfill Materials

There are four types of underfill materials commonly employed in IC packaging as shown in Table 2.2 [21].

Table 2.2 Four common types of underfill materials [21]

Name	Dispense Stage	Application Location	Fluxing ability	Material Form
Wafer level underfill	After IC fabrication and before wafer dicing	On the wafer	Yes	semi-solid (after B-stage)
No-flow underfill	Before chip assembly and reflow	On the substrate	Yes	liquid
Molded underfill	After chip assembly and reflow	Between chip and substrate, overmolding the chip	No	solid
Capillary underfill	After chip assembly and reflow	Between chip and substrate	No	liquid

Typical underfill materials consist of four parts, which will be described in details below:

(1) Epoxy resins:

Two carbon atoms and one oxygen atom form an oxirane ring. Epoxy resins are the molecules which possess the numbers of oxide rings > 2 as shown in Figure 2.9.

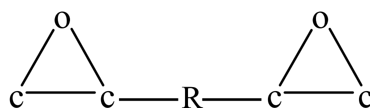

Figure 2.9 Structure of epoxy resins

Epoxy resins are liquid or solid at room temperature. With appropriate hardeners, epoxy resins can cure easily at the temperature ranging from 5 ℃ to 150 ℃ [22]. Ring

open polymerizations of oxirane rings are carried out with anions or cations. Figure 2.10 shows the curing mechanism of epoxy resins and Table 2.3 lists some common epoxy resins in commercial underfill materials. Cured epoxy resins possess many excellent properties described below [22]:

a. As the adhesive, cured epoxy resins possess hydroxyl groups to offer higher adhesive strength.

b. The shrinkage of epoxy resins is rare after curing reaction.

c. Cured epoxy resins are good insulators.

d. Cured epoxy resins possess excellent ability to resist alkali and acid.

e. After some modifications, epoxy resins can be utilized in many different applications

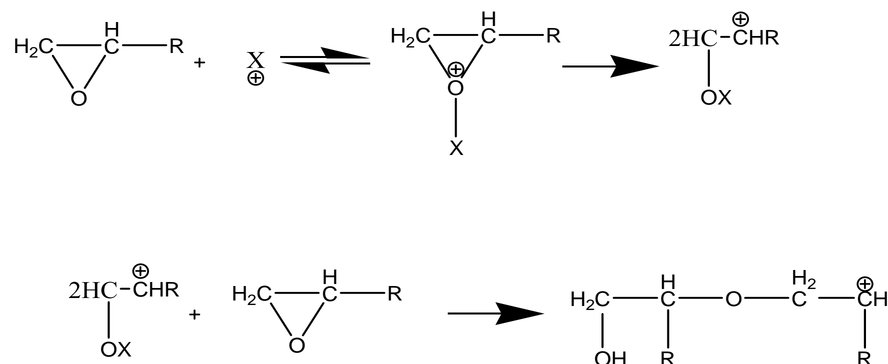

Figure 2.10 Curing mechanism of epoxy resins [22]

Table 2.3 Common epoxy resins [21]

Molecular structure	Synonym	Name
	EPON 828	diglycidyl ether of bisphenol-A epoxy resin
	EPON862	diglycidyl ether of bisphenol-F epoxy resin
	EPON SU-8	Epoxy phenol novolac resin
	ERL4221	cycloaliphatic epoxy resin

(2) Hardeners:

The curing reaction of epoxy resins needs hardeners to complete. There are many types of hardeners sorted by viscosity, curing temperature and time etc. Some common hardeners are shown in Figure 2.11.

(3) Catalysts:

The addition of catalysts can promote the curing reaction of epoxy resins and alter the curing temperature. Common catalysts are listed in Figure 2.11.

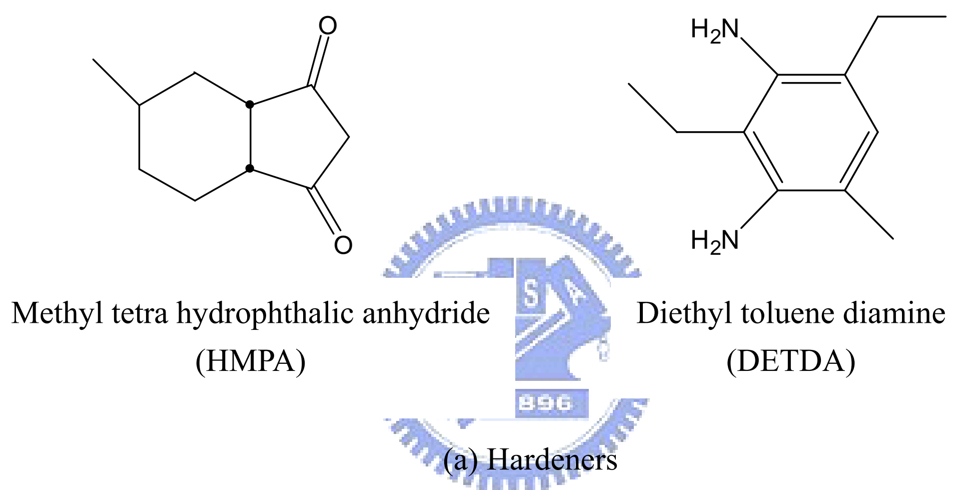

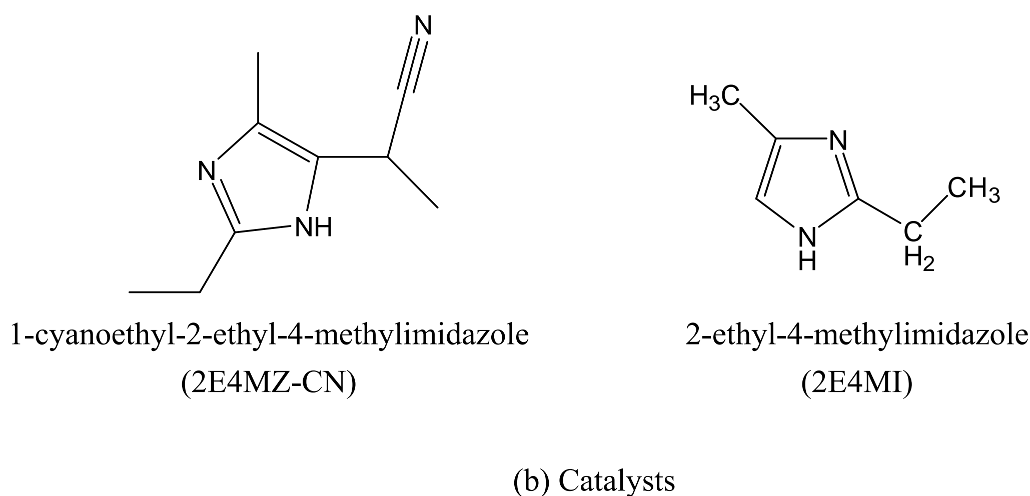

Figure 2.11 Common (a) hardeners and (b) catalysts in underfill materials [21]

(4) Fillers:

Fillers are usually employed to enhance the mechanical strength of underfill materials and reduce its coefficient of thermal expansion (CTE). The most commonly used filler in underfill materials is silica whose modulus is 76 GPa and CTE is 0.5 ppm/℃.

In this thesis, porous silica is utilized. It is obtained from the precursor, alkoxysilane $Si(OR)_4$, by sol-gel method. The method involves two steps [23-25]:

a. Hydrolysis reaction:

The hydrolysis reaction is carried out by $Si(OR)_4$ and H_2O molecules as shown in Figure 2.12.

b. Polymerization reaction:

After the hydrolysis reaction, the product will undergo the polymerization with an alkali catalyst as shown in Figure 2.13.

Finally, porous silica is obtained from the hydrolysis and polymerization reaction repeatedly. Porous silica obtained by sol-gel method possesses random pores.

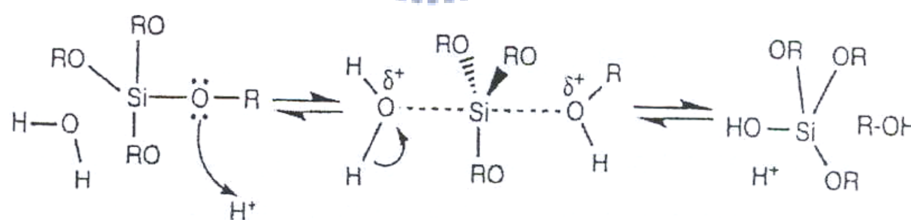

Figure 2.12 Hydrolysis reaction: $Si(OH)_4 + H_2O$

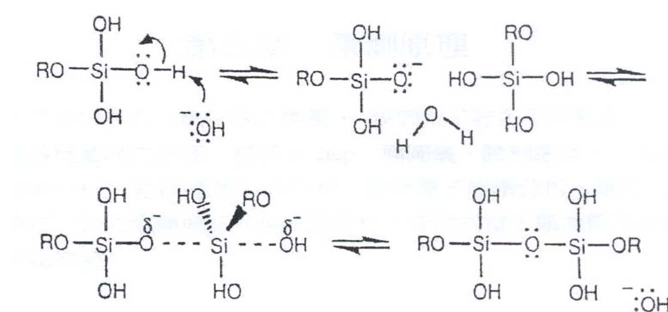

Figure 2.13 Polymerization reaction

2.3.2 Underfill materials and Low-K Flip Chip Packaging

Flip chip packaging offers so many merits that it becomes the one of the most attractive techniques in modern electronic packaging, including multi-chip modules (MCM) and high-frequency communications. The main function of the underfill materials is to protect the solder bumps from fatigue failure due to the thermal stress during the temperature cycling. The thermal-mechanical stress mainly arises from the coefficient of thermal expansion (CTE) mismatch between the silicon chip (2.5 ppm/℃) and the substrate (4–10 ppm/℃ for ceramics and 16 ppm/℃ for organic FR4 board). As a result, underfill materials provides an environmental protection to the solder joint to reduce the thermal stress on solder bumps and increase the solder joint fatigue life by orders of magnitude [19, 26].

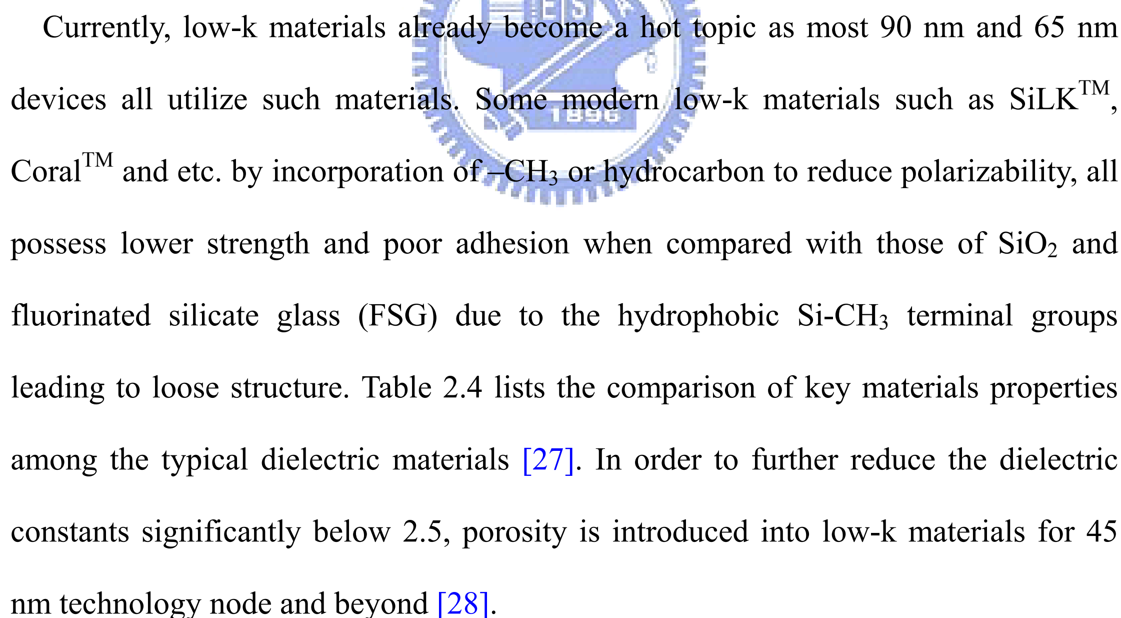

Currently, low-k materials already become a hot topic as most 90 nm and 65 nm devices all utilize such materials. Some modern low-k materials such as SiLK™, Coral™ and etc. by incorporation of $-CH_3$ or hydrocarbon to reduce polarizability, all possess lower strength and poor adhesion when compared with those of SiO_2 and fluorinated silicate glass (FSG) due to the hydrophobic Si-CH_3 terminal groups leading to loose structure. Table 2.4 lists the comparison of key materials properties among the typical dielectric materials [27]. In order to further reduce the dielectric constants significantly below 2.5, porosity is introduced into low-k materials for 45 nm technology node and beyond [28].

Due to the worse mechanical strength high CTE, low-k materials are prone to cracking and delamination [29]. Thereby, the reliability is of great concern for the flip chip packaging involving Cu/low-k die. Figure 2.14 illustrates the general structure of flip chip packaging involving low-k such as Coral™ in the backend interconnect.

Table 2.4 Properties of dielectric materials

Material property of dielectric materials

Items	Dielectric materials			
	SiO_2	FSG	SiLK	Coral
Process	CVD	CVD	Spin-on	CVD
Dielectric constant	3.9–4.1	3.5–3.7	2.6–2.8	2.7–2.9
Young's modulus[a]	1	0.85	0.04	0.19
Hardness[a]	1	0.95	0.05	0.27
CTE[a]	1	0.95	20.7	2.64

[a] Relative value.

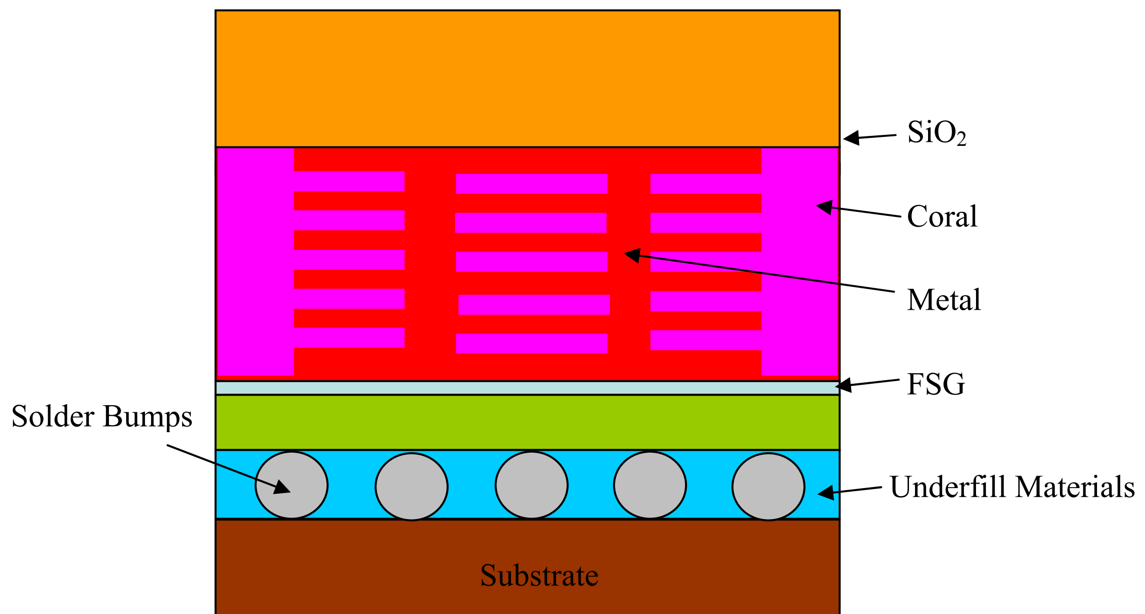

Figure 2.14 General structure of low-k flip chip package

The underfill materials must protect the solder bumps and the low-k layers from cracking and delamination. However, the properties of underfill materials capable of protecting both solder bumps and low-k layers simultaneously are conflicting. The reasons are articulated as follows [27, 29].

(1) Underfill materials with high modulus will transfer too much thermal mechanical stress, resulting from the CTE mismatch between the substrate and chip, to low-k layers. The stress will cause the crack and delamination of low-k layers as shown

in Figure 2.15 [27].

(2) Underfill materials with low modulus cannot sustain the thermal mechanical stress, resulting in the bump cracking as shown in Figure 2.16 [29].

Adequate underfill materials for flip chip packaging involving low-k should balance between the low-k chip shear stress and the solder bumps shear stress. As a result, underfill materials with immediate Tg (70-80℃) and moderate modulus (8-10 GPa), are optimum for flip chip packaging involving low-k interconnect. Finally, Figure 2.17 shows the directions of underfill materials development for different combination of ILD stress and solder fatigue [30].

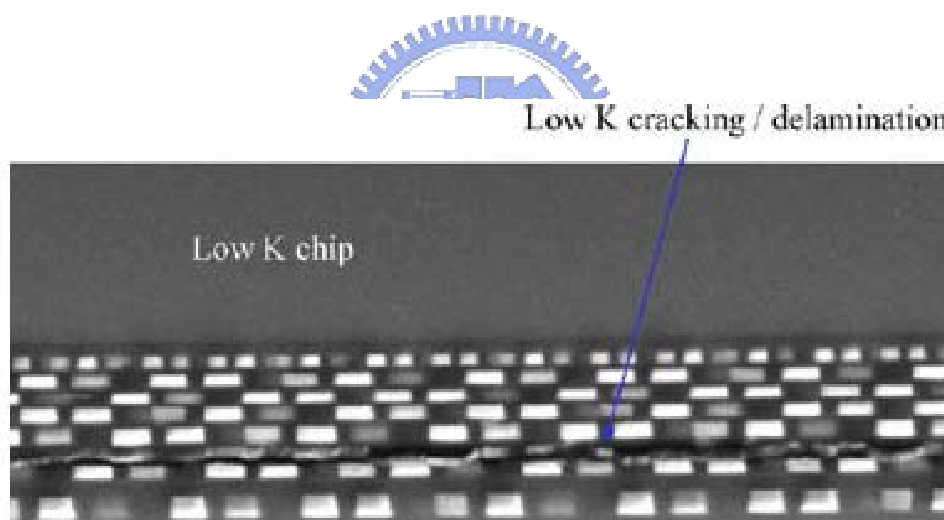

Figure 2.15 Crack and delamination of low-k layer [27]

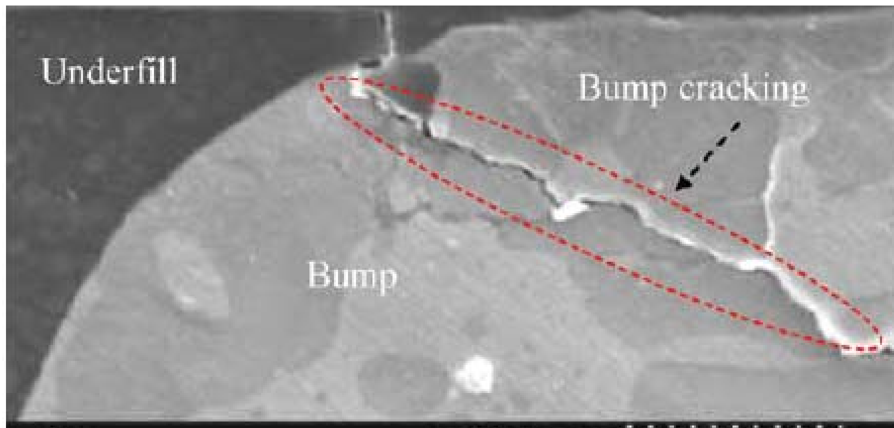

Figure 2.16 Bump cracking [27]

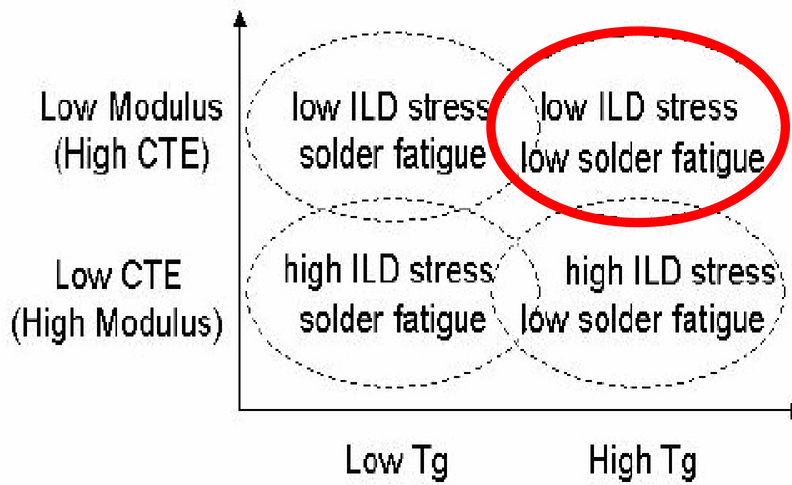

Figure 2.17 Directions of underfill materials development [30]

2.3.3 Underfill Materials and RF Electronic Packaging

2.3.3.1 RF Devices and Flip Chip Packaging

In the current microelectronic industry, high frequency device (RF device), operated at the frequency ranging from 0.1 to 100 GHz, has been widely used due to [8]:

(1) The development of microelectronic devices towards faster speed to transmit and handle signals.

(2) The growth of wireless communication applications.

Compared to the wire bonding and TAB technologies, flip chip packaging technology offers many advantages such as smaller size, higher I/O numbers, and better heat dissipation. Therefore, most RF devices are likely to employ flip chip packaging [31].

2.3.3.2 Underfill Materials for RF Devices

In RF devices, general underfill materials can offer excellent thermal-mechanical properties to protect the flip chip packaging. But, general underfill materials possess high dielectric constants above 3.5 which will result in a critical problem such as power consumption in RF applications, which is described in details below.

In RF flip chip packaging, how to decrease the power consumption, at high operating frequency is an important issue. Based on Equation (2.1) below, it is found that the power consumption of RF devices will rise due to increasing operating-frequency if the dielectric constant of underfill material is fixed.

$$P \infty 2\pi \cdot fV^{2}\varepsilon \cdot \tan\delta \quad (2.1)$$

where

P: power consumption

f: operated frequency

V: operated voltage

ε: dielectric constant

tan δ: dielectric loss

2.4 Motivation of Thesis

According to the previous sections, we realized that the underfill materials, utilized in the flip chip of RF devices, must possess not only good thermal-mechanical strength but also low dielectric constant. Underfill materials with low dielectric constants can improve the power consumption

The key components of underfill materials are epoxy resins and silica whose dielectric constants are 3.5 and 4.0, respectively. Consequently, the dielectric constants can be reduced by two methods listed as follows:

(1) To incorporate atoms and bonds which have lower polarizability

High electronic polarizability indicates that the materials have less tightly bound electrons, while low polarizability materials have tight binding of electrons. Lower polarizability can reduce dielectric constants [27]. Table 2.5 lists the electronic polarizability of several typical bondings.

Table 2.5 Electronic polarizability [27]

Bond	Polarizability (A^3)
C-C	0.531
C-F	0.555
C-O	0.584
C-H	0.652
O-H	0.706
C=O	1.02
C=C	1.643

According to the data above, it is indicated that C-C and C-F bonds have the lowest electronic polarizability which can be utilized for reducing dielectric constants of materials. For example, by replacing conventional bisphenol-A type epoxy resins with fluorinated epoxy resins as shown in Figure 2.18, the dielectric constants will decrease about 10 % due to CF_3 groups [34, 35]. Noticeably, although C-F bond can lower the dielectric constant, it may also degrade the adhesion strength of materials. In order to retain the desired and good properties of typical epoxy resins described in Section 2.3.1, the component of organic epoxy resins will not changed in this study.

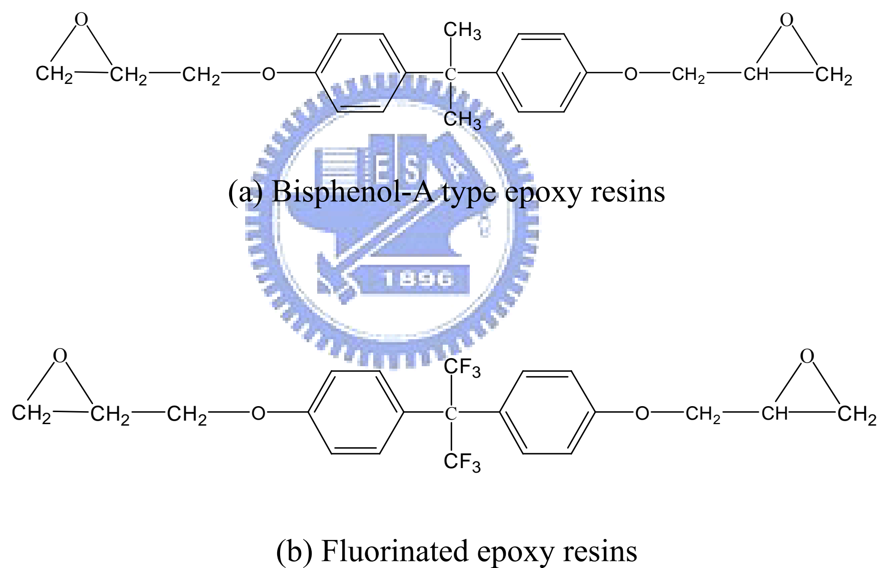

(a) Bisphenol-A type epoxy resins

(b) Fluorinated epoxy resins

Figure 2.18 Two epoxy resins: (a) bisphenol-A type epoxy resins (b)fluorinated epoxy resins

(2) To incorporate porosity into materials:

In order to further reduce RC propagation delay, it is necessary to use ultra low-k material (k < 2.5) as ILD (Interlayer dielectrics) for 65 nm or 45 nm node [36]. Many studies and researches on ultra-low-k materials have introduced pores

into the matrix because of the lowest dielectric constant of air (k_{vacuum} = 1). For porous low-k materials, the approach to generate porosity is to incorporate a templating agent or porogen (usually an organic compound) into materials and is later removed by thermal decomposition, leaving behind a void [37, 38] as shown in Figure 2.19.

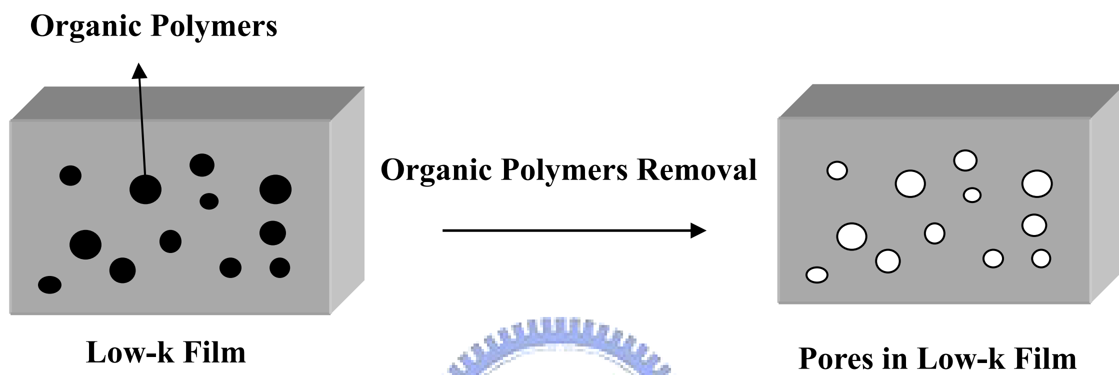

Figure 2.19 Incorporation of porosity into low-k layer

Based on the above-mentioned approaches for lower dielectric constants, the same concept of pore incorporation is adopted to achieve low-k underfill materials. Since the content of silica filler is up to 70 wt%, the dielectric constant of commercial underfill materials has a maximum value of 3.6 according to Equation (2.2) based on k_{SiO2} = 4.0 and k_{epoxy} = 3.1. If the organic part is introduced into 50% porosity, the dielectric constant will be decreased to 2.8. Similarly, if silica filler is introduced into 50% porosity, the dielectric constant will be decreased to 2.7. The method which introduces pores into silica filler can reduce the dielectric constant more due to higher volume fraction of silica filler in commercial underfill materials. In addition, common epoxy resins, such as bisphenol-A type epoxy resins, Bisphenol-F type epoxy resins, and cycloaliphatic epoxy resins, possess excellent adhesion and low viscosity [22].

Thus these epoxy resins as the organic component of underfill materials was utilized without alternation. Instead, pores and porosity was introduced into silica filler.

Therefore, in this thesis, porous silica was employed, replacing solid silica, to offer porosity for reducing dielectric constants. However, the pores would be back-filled with epoxy resins during the mixing and cure steps. How to protect the pores from the backfilling of epoxy resins was a critical issue. Therefore, an inorganic or organic, sacrificial material was employed to temporarily seal the interconnected pores in the porous silica at room temperature, and was later removed thermally during the crosslinking reaction of epoxy. Two types of porous silica were examined in this study; namely: (a) hollow zeeosphere with closed pores and (b) porous silica with open and interconnected pores.

The objectives of this thesis study were:

(1) To establish and characterize a pore-sealing technology to achieve the low-k underfill materials,

(2) To understand the mechanism of pore sealing, and

(3) To study the impact of pore-sealing pretreatments on the dielectric constants, and mechanical properties, and interfacial properties of low-k underfill materials.

$$LogK = \sum Vi \cdot LogKi \tag{2.2}$$

where

K: the dielectric constant of composite materials

Vi: the volume fraction of i-th component

Ki: the dielectric constant of i-th component

Chapter 3 Experimental

3.1 Sample Preparation

3.1.1 Chemicals

(1) Epikote™ 862 (Shell Co.) and Epikote™ 828 (Shell Co.):

The bisphenol-F and bisphenol-A epoxy resins were thermosetting polymer and employed as the matrix

(2) Methyl hexahydrophthalic anhydride (MEHHPA, CAS No. 19438-60-9, Sigma-Aldrich Co.):

MEHHPA was the hardener (crosslinking agents) to make the underfill materials harden fast.

(3) 2-Ethyl-4-Methylimidazole (2E4MI, CAS No 931-36-2, Sigma-Aldrich Co.) :

2E4MI was the catalyst to promote the crosslinking rate of underfill materials.

(4) Filler:

(a) Solid silica particles (Sumitomo Co.):

Solid silica was typically added to enhance the mechanical strength and lower the CTE of underfill materials. The average particle size of solid silica in this study was 5 μm.

2. Porous silica particles (CAS No. 112926, Sigma-Aldrich Co.):

The porous silica had porous structure whose particle size was 3 μm and the average pore size was 6 nm.

3. Zeeospheres (Peacco Enterprise Co.):

The zeeospheres were hollow silica-alumina spheres whose particle size was about 5 μm and the pore size was about 1.1 μm.

Figure 3.1 illustrated the chemical structures of the epoxides, catalyst and hardner.

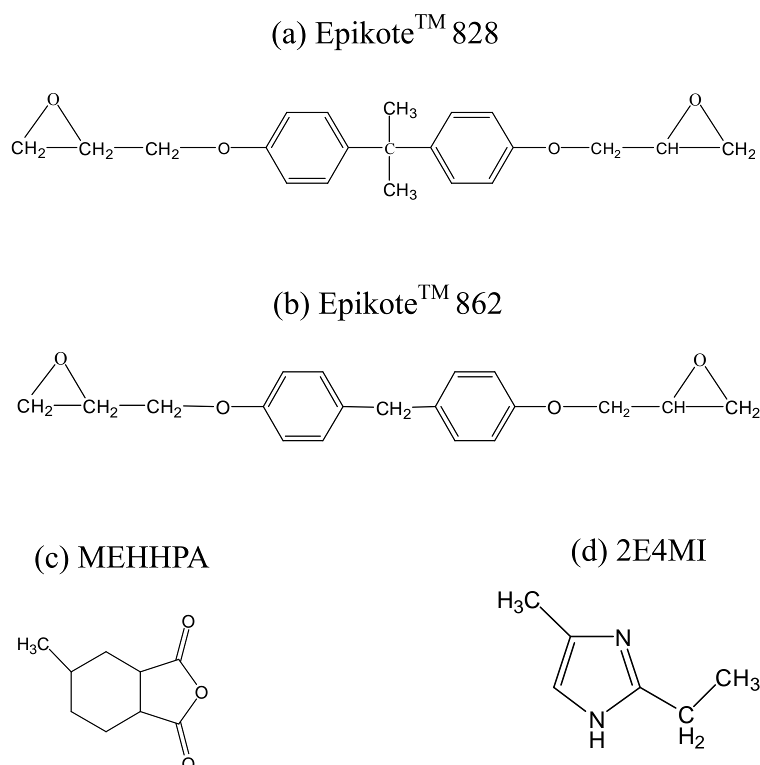

Figure 3.1 Chemical structures of (a) Epikote™ 828 (b) Epikote™ 862 (c) MEHHPA (d) 2E4MI

3.1.1.1 Pore-Sealing Pretreatment

A pore-sealing pretreatment for porous silica was developed because the epoxy resins possessed fluidity at room temperature and easily fill the pores of porous silica fillers by capillary force. The pore volume of porous silica must be retained until the completion of curing reaction to achieve low-k underfill materials. Therefore, organic or inorganic sacrificial materials were employed to temporarily seal the interconnected pores in porous silica and removed thermally during the crosslinking reaction. In the thesis, two materials were used as the pore-sealing materials for porous silica fillers.

(1) N-butanol (CAS No. 71-36-3, Sigma-Aldrich Co.)

(2) Hexamethylcyclotrisiloxane (D3) (Shin-Etsu Silicone Taiwan Co.)

During the pore-sealing pretreatment, porous silica mixed with N-butanol at room temperature or D3 in liquid phase at 95℃. Then, by concentration gradient and capillary force, N-butanol and D3 were absorbed by porous silica and sealed the pores. After the mixture was cooled down, the rest of formulation such as epoxides, hardner, and catalyst was then mixed.

3.1.2 Preparation of underfill materials

There were two kinds of underfill materials studied in this thesis. One was conventional capillary underfill materials and the other was low dielectric constant (low-k) underfill materials. The formulation of the capillary underfill material was listed in Table 3.1.

In order to obtain underfill materials with low dielectric constants, we introduced porosity (k_{vacuum} = 1) into underfill materials. The low-k underfill materials had the same organic parts as the capillary underfill; however, the solid silica was replaced with zeeospheres or porous silica. Table 3.2 listed low-k underfill materials in this thesis without pore-sealing pretreatment, while Table 3.3 listed low-k underfill materials with pore-sealing pretreatment by N-butanol or D3.

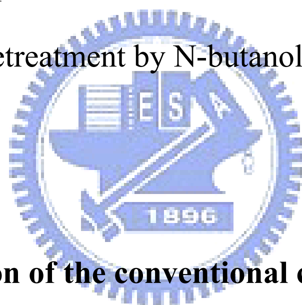

Table 3.1 Formulation of the conventional capillary underfill material

	Conventional capillary underfill
Organic part (85 wt%)	Epikote™ 828 Epikote™ 862 MEHHPA 2E4MI
Filler (15 wt%)	Solid silica particles

Table 3.2 Formulations of low-k underfill materials A and B, without pore-sealing pretreatment

	Low-k underfill material A	Low-K underfill material B
Organic part (85wt%)	Epikote^{TM} 828 Epikote^{TM} 862 MEHHPA 2E4MI	Epikote^{TM} 828 Epikote^{TM} 862 MEHHPA 2E4MI
Filler (15wt%)	Zeeospheres	Porous silica without pore-sealing pretreatment

Table 3.3 Formulations of the low-k underfill materials C, D, and E, with pore-sealing pretreatment

	Low-K underfill material C	Low-K underfill material D	Low-K underfill material E
Organic part (85 wt %)	Epikote^{TM} 828 Epikote^{TM} 862 MEHHPA 2E4MI	Epikote^{TM} 828 Epikote^{TM} 862 MEHHPA 2E4MI	Epikote^{TM} 828 Epikote^{TM} 862 MEHHPA 2E4MI
Filler (15 wt %)	Porous silica	Porous silica	Porous silica
Pore-sealing material	D3	D3	N-butanol
Porous silica: pore sealing material ratio (weight)	1:1	1:3	n/a

3.1.2.1 Curing Profiles of Underfill materials

Differential scanning calorimetry (DSC, PerkinElmer Diamond) was employed to determine the curing profiles of underfill materials in this thesis. From the DSC curve of conventional capillary underfill material as shown in Figure 3.2, it was found that the conventional capillary underfill began to cure at 120 ℃ and reached the full acutest degree of curing reaction at 145 ℃. Based on the thermal reactivity, we defined the curing profile involving two steps: (1) heating from room temperature to 150 ℃ with a 5 ℃/min heating rate, and then (2) isothermal heating at 150 ℃ for 2 hours.

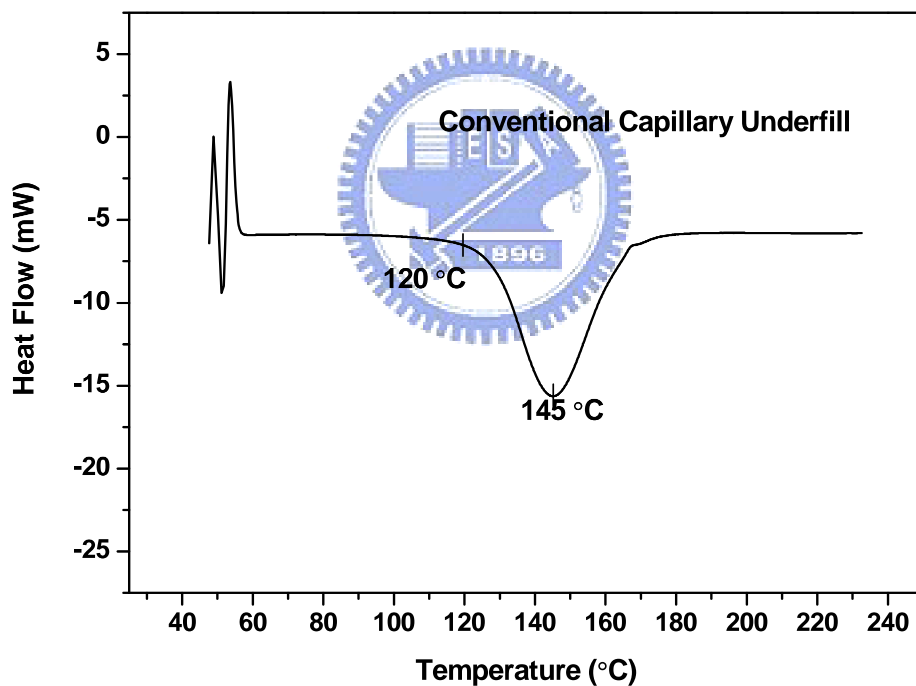

Figure 3.2 DSC curve of conventional capillary underfill

Figures 3.3 (a) and 3.3 (b) were the DSC curves of low-k underfill material A and low-k underfill material B, respectively. From the thermal reactivity, it indicated that low-k underfill material A began curing reaction at 120 ℃ and then reached the

highest degree of curing reaction at 150℃, while low-k underfill material B started curing reaction at 125 ℃ and then reached the highest degree of curing reaction at 165 ℃. Even though the organic parts of these underfill materials were all the same, the curing temperature of low-k underfill materials was obviously higher than that of conventional capillary underfill or low-k underfill material A. Compared to solid silica and zeeospheres, porous silica easily trapped the epoxy resins due to its open pores. As a result, for low-k underfill material B, these interconnected, open pores hindered the curing reaction such that the temperature range was increased. Based on the DSC curves, the curing profile of low-k underfill material A involved the following two steps: (1) heating from room temperature to 155 ℃ with a 5 ℃/min heating rate, and (2) isothermal heating at 155 ℃ for 2 hours. In contrast, the other curing profile of low-k underfill material B involved: (1) heating from room temperature to 170 ℃ with a 5℃/min heating rate, and (2) isothermal heating at 170 ℃ for 2 hours.

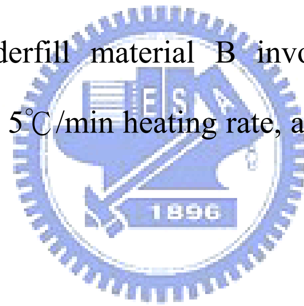

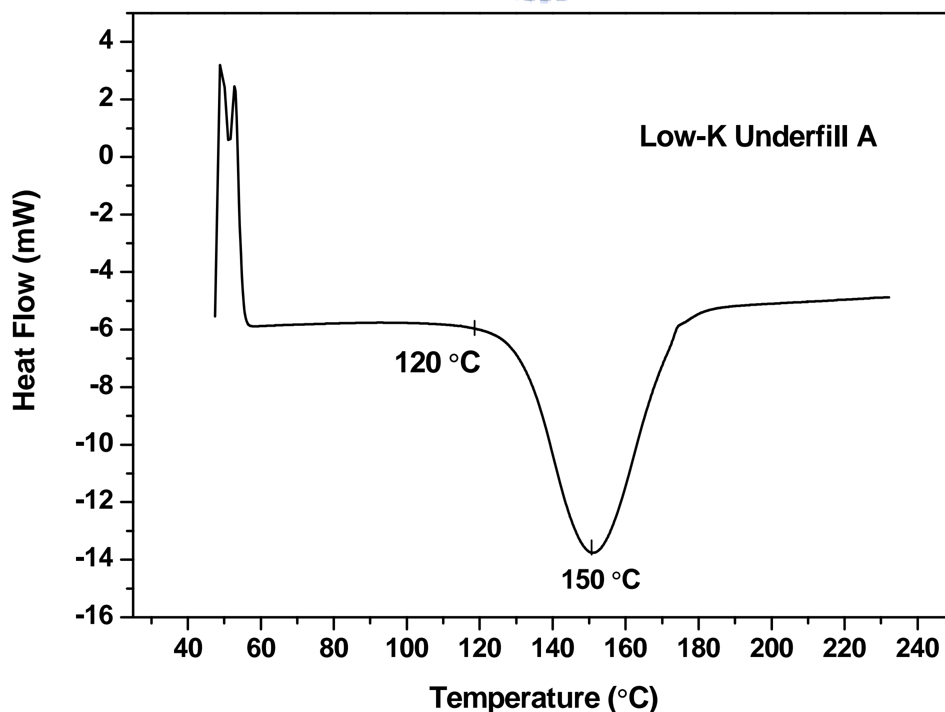

(a) DSC curve of low-k underfill material A

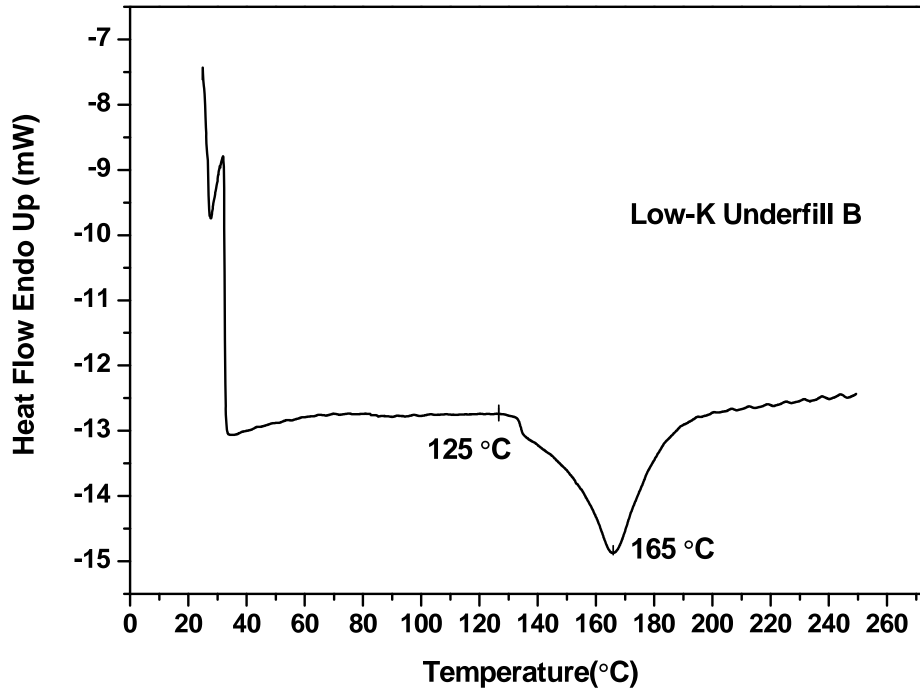

(b) DSC curve of low-k underfill material B

Figure 3.3 DSC curves of (a) low-k underfill material A and (2) low-k underfill material B

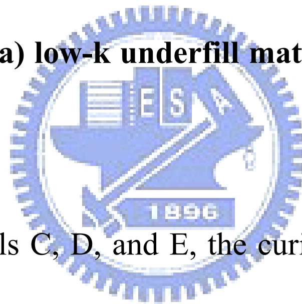

For low-k underfill materials C, D, and E, the curing profile was similar to low-k underfill material B; besides, a specific step was used in the curing profile to remove the pore-sealing materials, N-butanol or D3. The curing profile involved: (1) heating from room temperature to 120℃ with a 5 ℃/min heating rate, (2) isothermal heating at 120℃ for 10 ~ 20 mins while the chamber was pumped to low pressure, (3) heating from 120℃ to 170℃ at a 5℃/min heating rate, and then (4) isothermal heating at 170 ℃ for 2 hours.

3.2 Experimental Approaches

In this thesis, both capillary underfill and low-k underfill materials used the same organic components: epoxy resins, hardener and catalyst. The differences were the filler types which included solid silica, zeeospheres, and porous silica. There were three types of underfill materials involving (1) conventional capillary underfill with solid silica as fillers (15 wt%) (2) low-k underfill with zeeosphere as fillers (15 wt%), and (3) low-k underfill with porous silica as fillers (15 wt%).

The filler type which involved solid silica, zeeospheres and porous silica. Noticeably, the surface area of porous silica was up to 300 m^2/g. Because of such high surface area, the porous silica fillers without pore-sealing pretreatment would cause the viscosity of underfill materials increased drastically. As the amount of porous silica was up to 50 ~ 70 wt% like commercial underfill materials, excess pure porous silica would result in high-viscosity, non-fluidity of underfill materials. In order to prevent such problem, the amount of fillers for all the underfill formulations in this study was limited at 15 wt%. The entire experimental procedures could be summarized in the flow chart as illustrated in Figure 3.4, which involved the following key experiments:

1. DSC and rheometer were employed to select the appropriate pore-sealing materials.
2. Pore-sealing pretreatment was carried out on porous silica.
3. SEM and BET methods were utilized to study the pore size distribution, morphology, and the effect and mechanism of pore-sealing pretreatment.
4. Measurement of dielectric constants and moduli of various underfill materials.

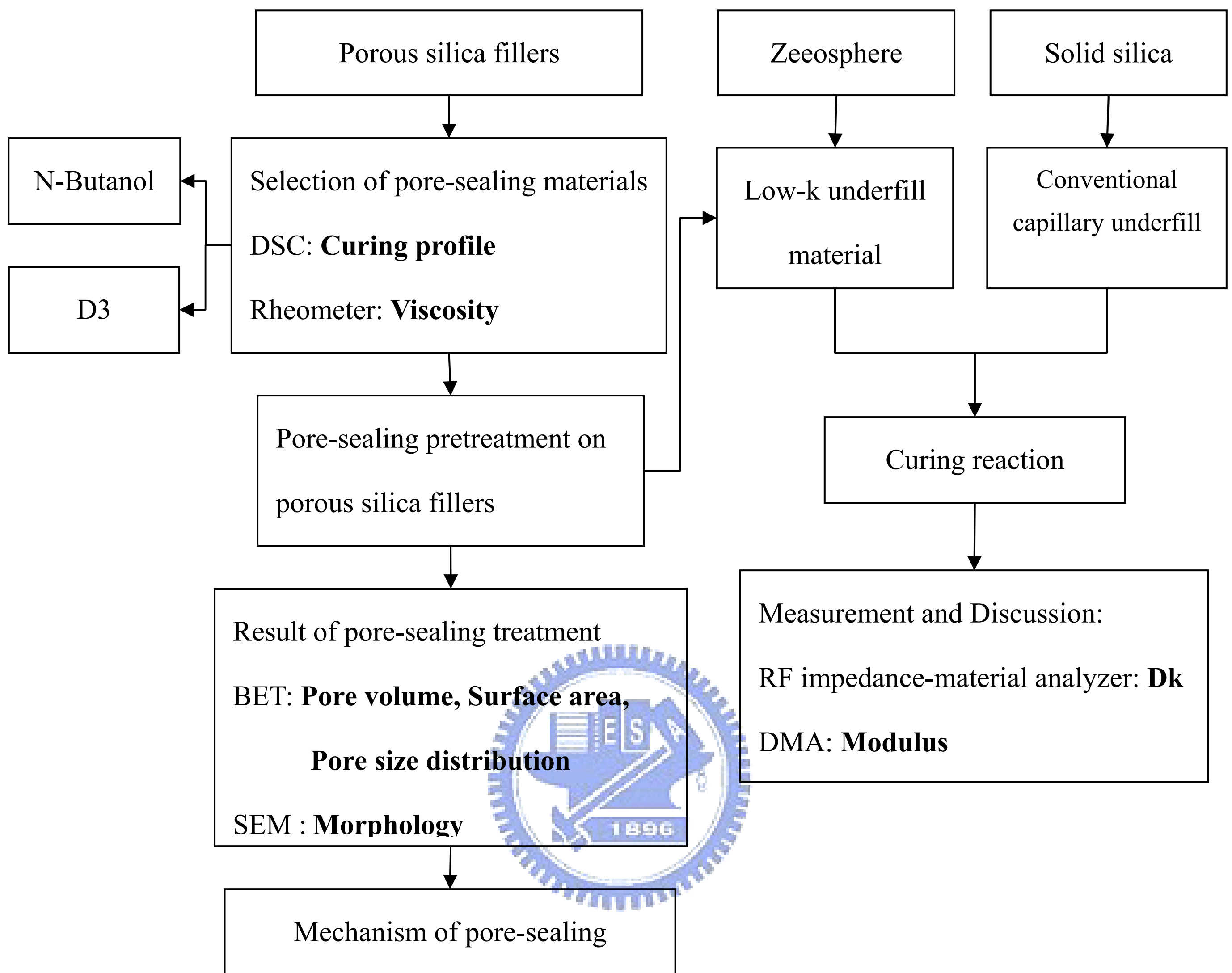

Figure 3.4 Flow-chart of experimental procedures

3.3 Instrumentation

3.3.1 Differential Scanning Calorimetry (DSC) [39]

The principle of differential scanning calorimetry (DSC) is to measure the energy variation of the sample affected by temperature. However, there are two types of differential scanning calorimetry (DSC) according to different designed modes:

(1) Heat Flux DSC [39]

The designed mode of heat flux DSC is shown in Figure 3.5. The sample and reference are put in two sample holders which are heated by the same heat source. The two sample holders have individual thermocouples to measure the temperature of the sample and reference. There is a temperature difference (ΔT) between the sample and reference during heating or cooling due to the endothermic or exothermic reactions of the sample. Heat flux DSC measures the ΔT continuously and transforms ΔT into the energy variation (ΔQ) to show. The ΔQ inaccuracy of heat flux DSC is within ± 5%.

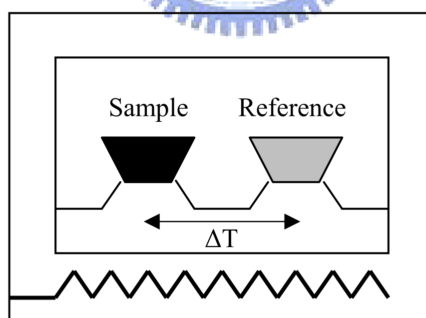

Figure 3.5 Heat Flux DSC [39]

(2) Power Compensation DSC [39]:

Figure 3.6 is the designed mode of power compensation DSC. The sample and reference are put in two individual Pt-Lr heating furnaces. The furnaces have individual Pt heating wires and Pt resistance temperature detector (PRTD). Pt heating wires offers energy precisely and fast. PRTD has linear relationship

between resistance (Ω) and temperature (-250℃~900℃). PRTD can measure the temperature of the sample and reference by measured Ω. There is a resistance difference (ΔΩ) between the sample and reference during heating or cooling due to the endothermic or exothermic reactions of the sample. Subsequently, Pt heating wires offer additional energy (ΔQ) fast to compensate the energy difference and make the sample and reference have the same Ω. The ΔQ inaccuracy of power compensation DSC was about ± 1%.

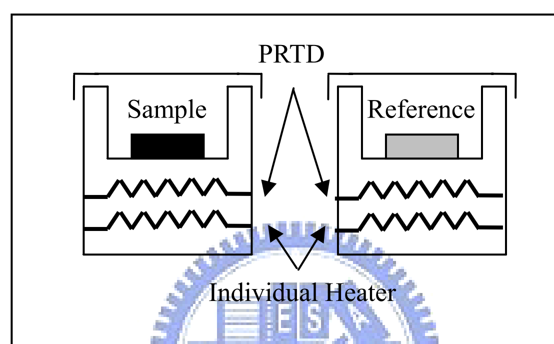

Figure 3.6 Power Compensation DSC [39]

In this thesis, DSC was employed to investigate the curing reaction of underfill materials. The uncured underfill materials samples (5~10 mg) was placed in a Pt holder for DSC measurement using a PerkinElmer Diamond DSC in power compensation mode. Finally, Figure 3.7 illustrates the typical DSC curves of some typical polymer transitions.

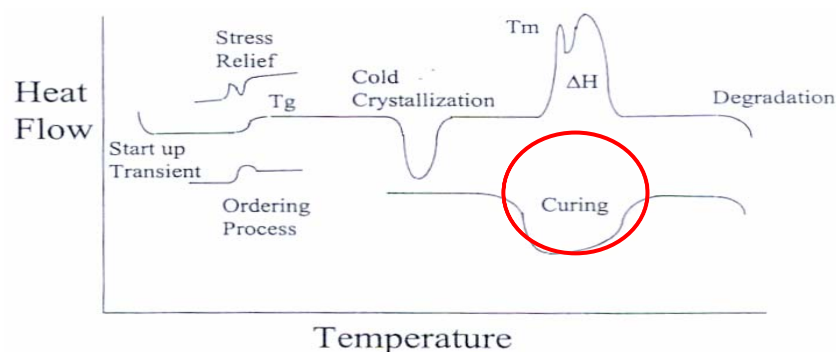

Figure 3.7 Typical DSC curves of some general polymer transitions

3.3.2 Rheometer [40]

A TA Rheometer 1000 was employed to measure the viscosity as a function of temperature. Typically, the uncured underfill material sample of about 10 ~ 20 g was placed in an aluminum holder for rheometer measurement. Figure 3.8 showed the structure of the rheometer. The principal advantages of this rheometer include that loading and cleaning are simple and the shear rate is uniform. During the measurement, the plate is fixed while the cone is rotated by torque. From the rotating rate and torque, the viscosity can be obtained.

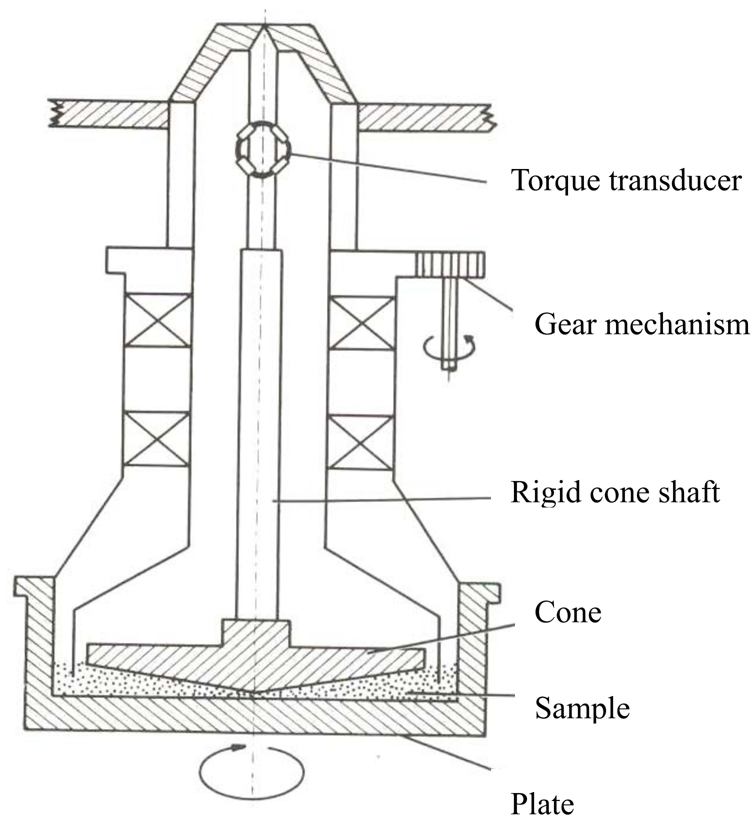

Figure 3.8 Structure of rheometer [40]

To derive an expression relating the shear rate in the space between the cone and the plate to the rotational speed and cone angel, the following assumptions are made.

(1) At sufficiently low rotational speeds, the acceleration terms of the motion can be neglected

(2) The cone angle is very small so that certain trigonometric relationships can be used to simplify equations.

(3) The free surface of liquid at the edge of the gap between the cone and the plate is spherical shape with a radius of curvature equal to the cone radius, and the flow is uniform right up to the surface. Therefore, edge effects are neglected.

(4) The surface tension operating at the free surface doesn't affect the fluid motion.

When these assumptions are valid, the viscosity (η) can be calculated from Equations (3.1) ~ (3.3) below [40].

$$\gamma = \frac{\Omega}{\theta} \tag{3.1}$$

$$M = \frac{2}{3}\pi R^3 \tau \tag{3.2}$$

$$\eta = \frac{\tau}{\gamma} = \frac{3M\theta}{2\pi R^3 \Omega} \tag{3.3}$$

where

η: viscosity

M: torque amplitude

θ: cone angle

R: cone radius

Ω: rotation speed

3.3.3 Brunauer-Emmett-Teller gas adsorption method (BET) [41]

A Quantachrome NOVA-1000A based on Brunauer-Emmett-Teller method (BET) absorption method was employed to measure the surface area, pore volume, and pore size distribution using a nitrogen gas. The sample typically contained about 30 ~ 50 mg in powder form. The principle of BET method is based on Langmuir Equation (3.4) [41].

$$\frac{P}{C_s} = \frac{P}{C_{sm}} + \frac{1}{BC_{sm}} \tag{3.4}$$

where

P: partial pressure of adsorptive phase

C_s: concentration of adsorptive phase at any moment

C_{sm}: concentration of monolayer adsorption

B: constant

Finally the Brunauer-Emmett-Teller Equation (3.5) is obtained by extending Langmuir equation [41] from monolayer adsorption to multilayer adsorption.

$$\frac{P}{V(P_0 - P)} = \frac{1}{V_m C} + \frac{(C-1)P}{V_m P_0} \tag{3.5}$$

where

P: partial pressure of adsorptive gas

V: volume of adsorptive gas at P partial pressure

V_m: volume of adsorptive gas for monolayer

P_0: saturation pressure of adsorptive gas

C: constant

From Equation (3.5), we can get V_m. Finally, the surface area (S) of the sample is obtained from Equation (3.6) by V_m [41].

$$S = \frac{V_m N \alpha}{W} \tag{3.6}$$

where

S: surface area of sample

N: Avogadro's number

α: covered area of adsorptive gas ($16.2*10^{-20}$ m^2/molecule of nitrogen molecule)

W: weight of sample

In addition, pore size and distribution of the sample can be obtained by Equation (3.7) [41].

$$d = \frac{4V}{S} \tag{3.7}$$

where

d: average pore size

V: volume of adsorptive gas

S: surface area of sample

Pores can be classified by pore size as follows:

(1) Micropores with dimensions < 2 nm

(2) Mesopores with dimension 2-50 nm

(3) Macropores with dimension >50 nm

Figure 3.9 showed the typical BET curves of these pores [41].

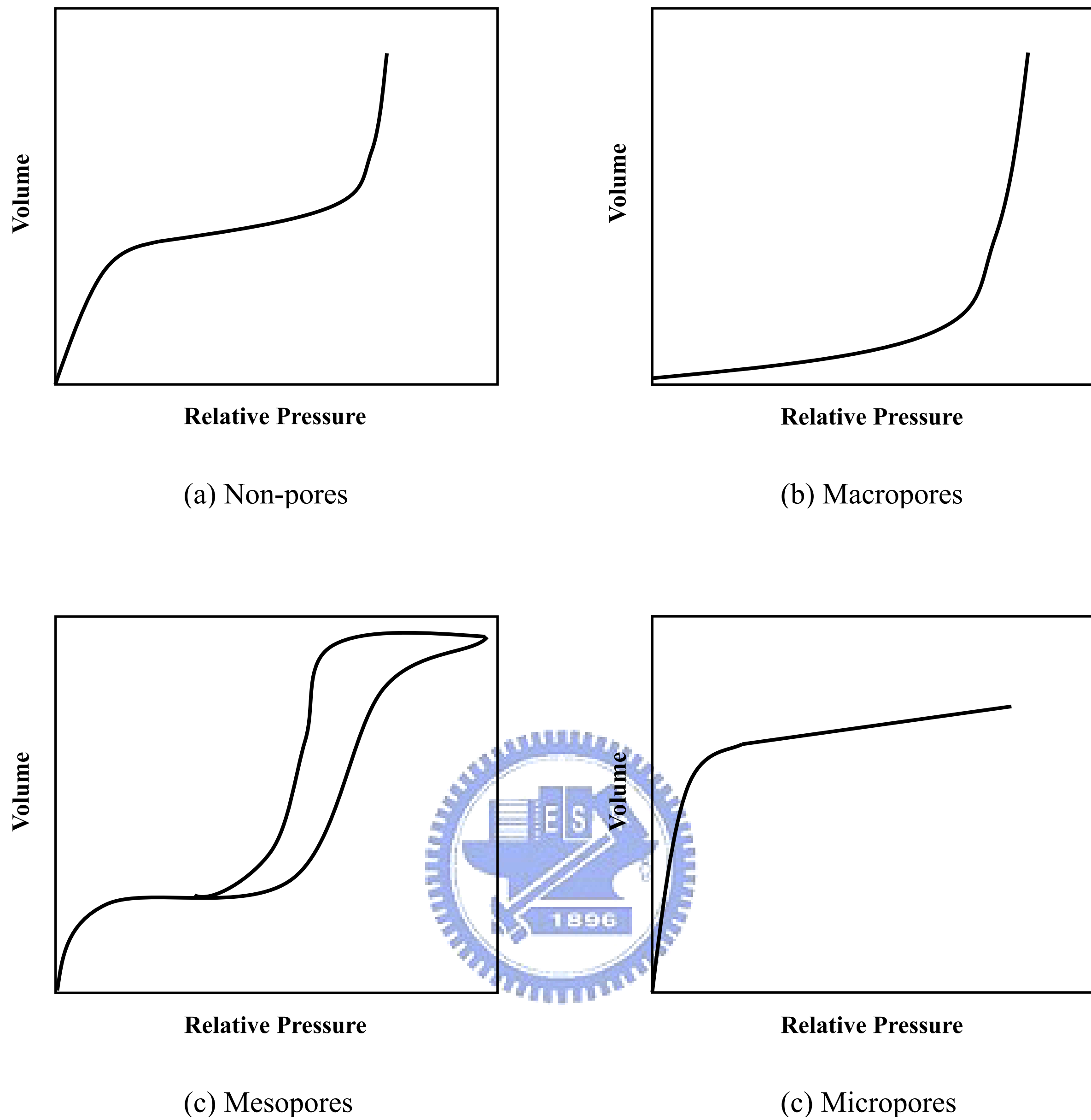

Figure 3.9 Typical BET curves : (a) non-pores (b) macropores (c) mesopores (d) micropores

3.3.4 RF Impedance-Material Analyzer

A HP 4291B RF impedance material analyzer with broad frequency range (1 MHz ~ 1.8 GHz) was employed to measure the relative permittivity (or dielectric constant) of a plate shaped, solid dielectric material. The relative permittivity can be calculated by the Equation (3.8) [42].

$$\varepsilon_r = \frac{Yd}{j\omega\varepsilon_0 S} \tag{3.8}$$

where

ε_r: relative permittivity

Y: measured admittance

ε_0: permittivity of free space

d: height of the sample

S: area of the lower electrode

A fully cured, underfill material sample with a thickness of about 2 mm was used for the dielectric constant measurement at 1GHz.

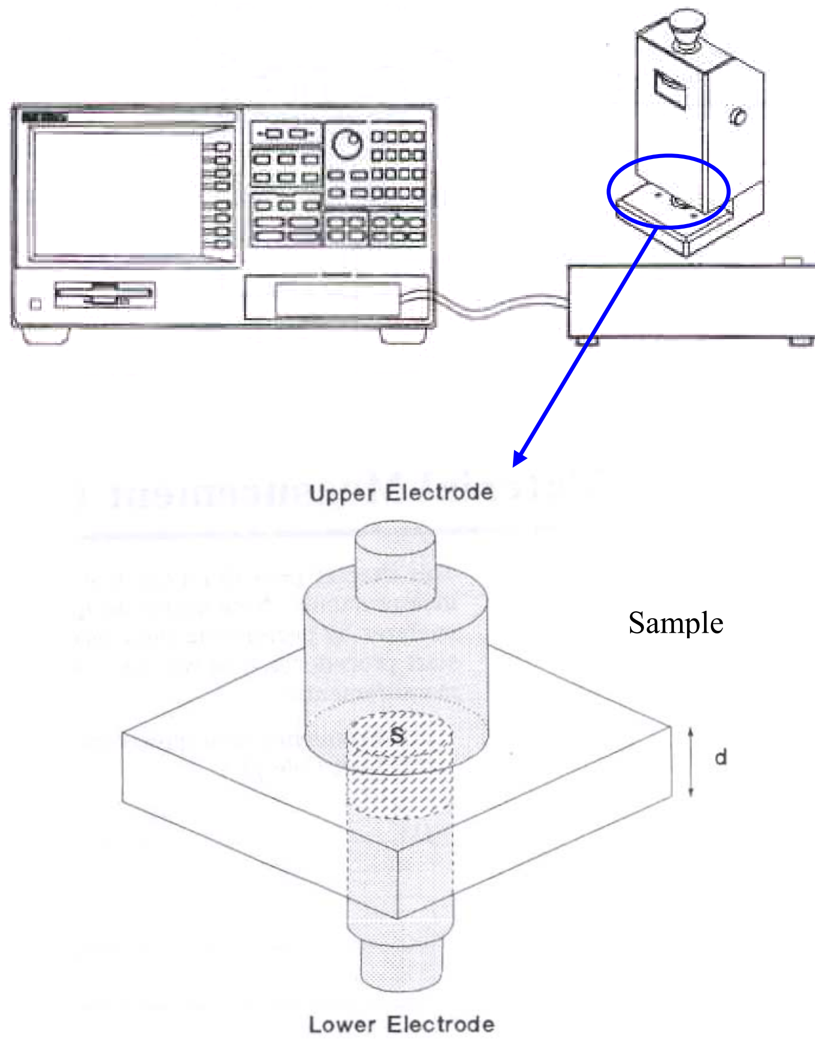

Figure 3.10 RF Impedance/Material Analyzer [42]

3.3.5 Dynamic Mechanical Analyzer (DMA)

3.3.5.1 Fundamental Theory

The operating principle of dynamic mechanical analyzer (DMA) as shown in Figure 3.11 can be simply described as applying an oscillating force to a sample and analyzing the response to that force. Materials' response includs phase-lag (δ) and amplitude [43]:

(1) Phase-Lag (δ):

When DMA applies a stress (σ) on a material, the delayed strain (ε) of material's response is the phase-lag (δ). Typical materials are between full elasticity and full viscosity. The viscosity property of a material results in the phase-lag (δ).

(2) Amplitude:

In addition to the phase-lag (δ), the amplitude also changes. The amplitude arises from the elasticity property of materials and fits Hook's Law. We can calculate the modulus by the amplitude.

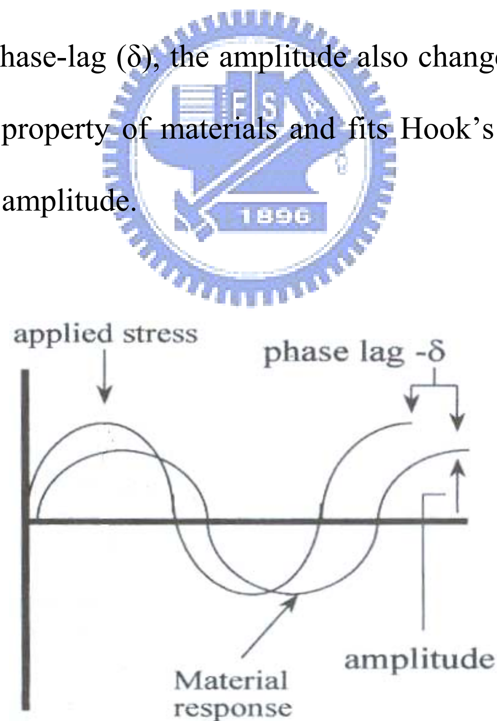

Figure 3.11 The response of materials in DMA

In the dynamic mechanical analyzer (DMA), the stress (σ) is known and the strain (ε) is measured. According to phase-lag (δ) and amplitude, we can get the storage

modulus (E’) and loss modulus (E’’) respectively by Equations (3.9) and (3.10).

$$E' = (\sigma / \varepsilon) \cdot \cos\delta \qquad (3.9)$$

$$E'' = (\sigma / \varepsilon) \cdot \sin\delta \qquad (3.10)$$

where

σ: applied stress

ε: strain

δ: phase-Lag

By the storage modulus (E’) and loss modulus (E’’), we can obtain the damping (tanδ) from Equation (3.11).

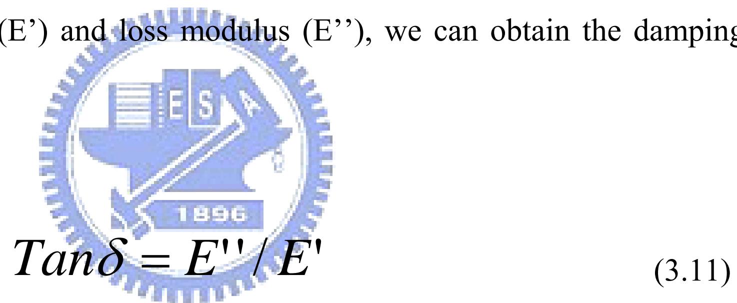

$$Tan\delta = E'' / E' \qquad (3.11)$$

where

E’: storage modulus

E’’: loss modulus

The value of tanδ is the degree of absorbed energy in materials. The larger tanδ represents the more energy absorbed in the sample.

3.3.5.2 Characterization of Adhesion

It has been found the energy was dissipated at the interface between fillers and matrix if the adhesion was poor. The relationship between the energy loss and adhesion is characterized by tanδ as shown in Equation (3.12) and (3.13) [44].

$$Tan\delta_{adh} = Tan\delta_{\exp} - Tan\delta_{s} \tag{3.12}$$

where

$Tan\delta_{adh}$: internal energy dissipation

$Tan\delta_{exp}$: measured loss tangent of composite materials

$Tan\delta_{S}$: effective loss tangent for perfect adhesion of composite materials

$$Tan\delta_{s} = \frac{Tan\delta_{f} E_{f} V_{f} + Tan\delta_{m} E_{m} V_{m}}{E_{m} V_{m} + E_{f} V_{f}} \tag{3.13}$$

where

E_f: modulus of fillers

V_f: volume fraction of fillers

$Tan\delta_f$: loss tangent of fillers

E_m: modulus of matrix

V_m: volume fraction of matrix

$Tan\delta_m$: loss tangent of matrix

In a two-component composite system, the energy dissipation $Tan\delta_{adh}$ arises from the poor adhesion. Since $Tan\delta_s$ is fixed in the same composite system, higher $Tan\delta_{exp}$ results in larger $Tan\delta_{adh}$, indicating that more energy is dissipated due to poor adhesion.

In this study, a PerkinElmer DMA 7 was employed to measure the elastic modulus of cured underfill materials and the loss factor, tanδ of the composite system in the underfill materials at 40 ^{o}C. The strip sample of cured underfill materials had the dimension of 25 mm × 6 mm × 2 mm.

Chapter 4 Results and Discussion

4.1 Selection of pre-sealing materials by thermal reactivity and viscosity

Since epoxy resin possessed fluidity prior to curing reaction, it can easily fill the pores in porous silica fillers by capillary force when underfill formulation was prepared. In order to reduce the dielectric constant of underfill material, the pore volume of porous silica must be occupied by a pore-sealing material temporarily, which would be removed at the enod of curing step. DSC and rheometer were first employed to examine the curing profile and the viscosity of low-k underfill material B.

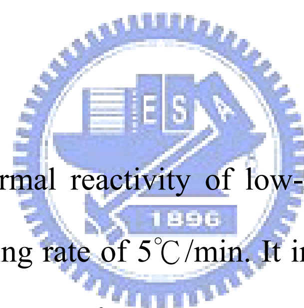

Figure 4.1 showed the thermal reactivity of low-k underfill material B by DSC from 30℃ to 250℃ at a heating rate of 5℃/min. It indicated that the low-k underfill material B started crosslinking at 125℃ and reached the full acutest degree of curing reaction at 165℃. Then, Figure 4.2 showed the viscosity variation of low-k underfill material B. By combining the viscosity variation with DSC curve above, from 115 ℃ to 165 ℃, it indicated that viscosity of low-k underfill material B dropped steadily even the epoxy resins started to cure at 125 ℃, which resulted from the heat energy to make epoxy resins still possess higher mobility and fluidity. As curing reaction continued, epoxy resins formed more and more network structures which would inhibit their movement. Therefore the degree of curing reaction reached the acutest degree at 165 ℃ and simultaneously the viscosity began to increase drastically and fast.

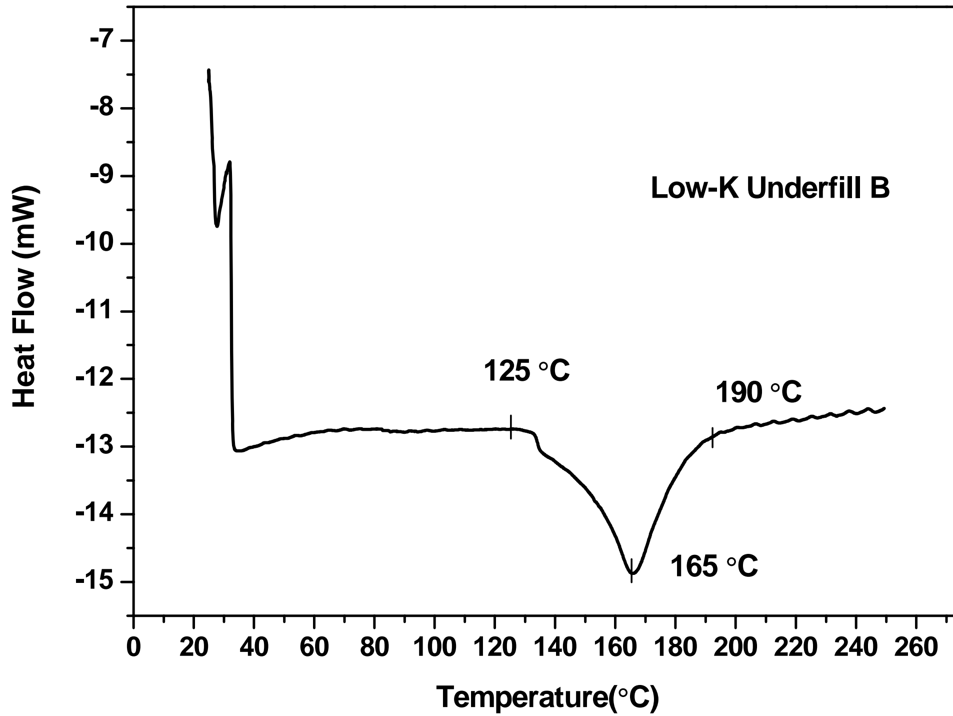

Figure 4.1　DSC curve of low-k underfill material B without pretreatment

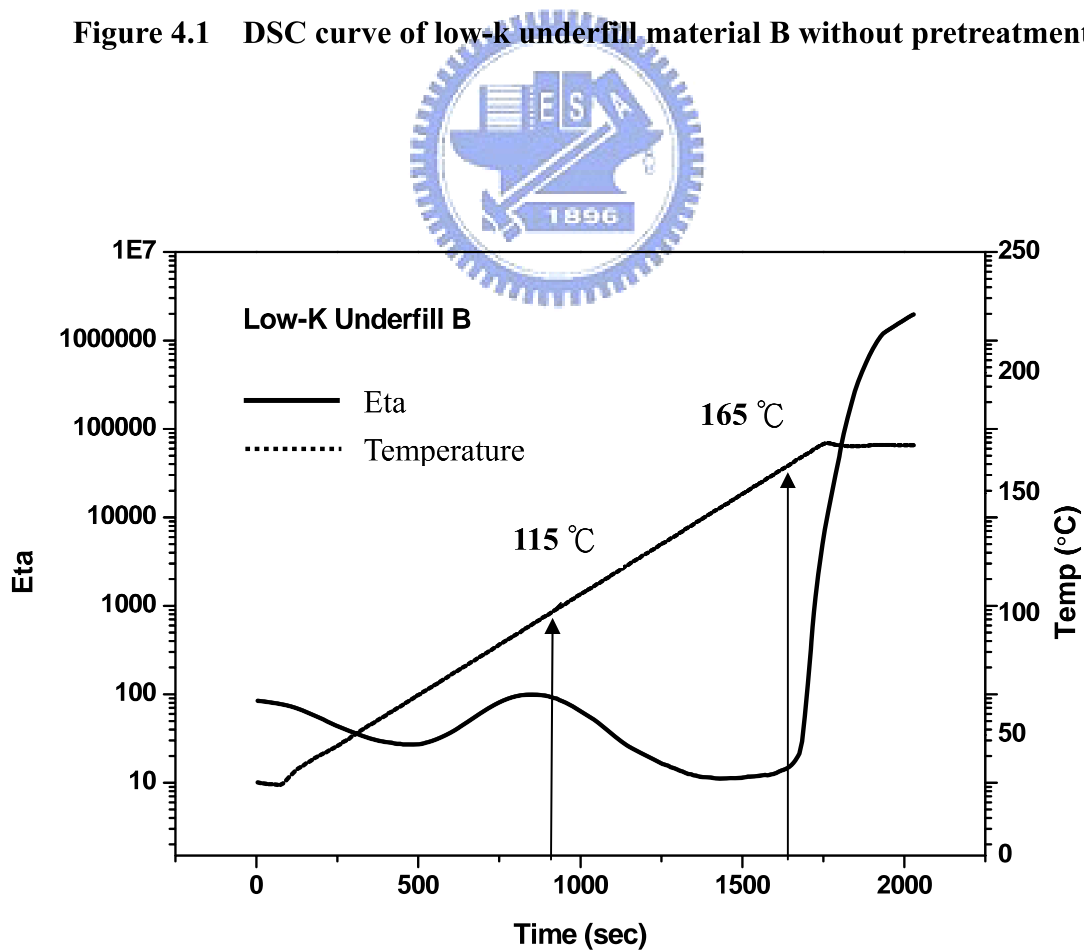

Figure 4.2　Viscosity as a function of temperature for low-k underfill material B

Based on the relationship between thermal reactivity and viscosity variation of low-k underfill material B, materials with boiling temperature at 120-140 ℃ could serve as sacrificial materials to seal the pores of porous silica fillers and hinder the reflow of epoxy resins back to the pores by its vapor outgassed from the sealed pores until the completion of curing reaction.

Besides the proper boiling point ranging from 120 to 140℃, the other requirements of pore-sealing materials were:

(1) Poor compatibility:

The materials shall possess poor compatibility with epoxy resins such that hindered the backflow of epoxy resins into the pores

(2) Molecular size:

The size of pore-sealing material must be smaller than the average pore size of porous silica (6 nm) in order to easily enter the pores for sealing them.

Based on these requirements, N-butanol and Hexamethylcyclotrisiloxane (D3), shown in Figure 4.3, were chosen to carry out pore-sealing pretreatments of porous silica in low-k underfill materials.

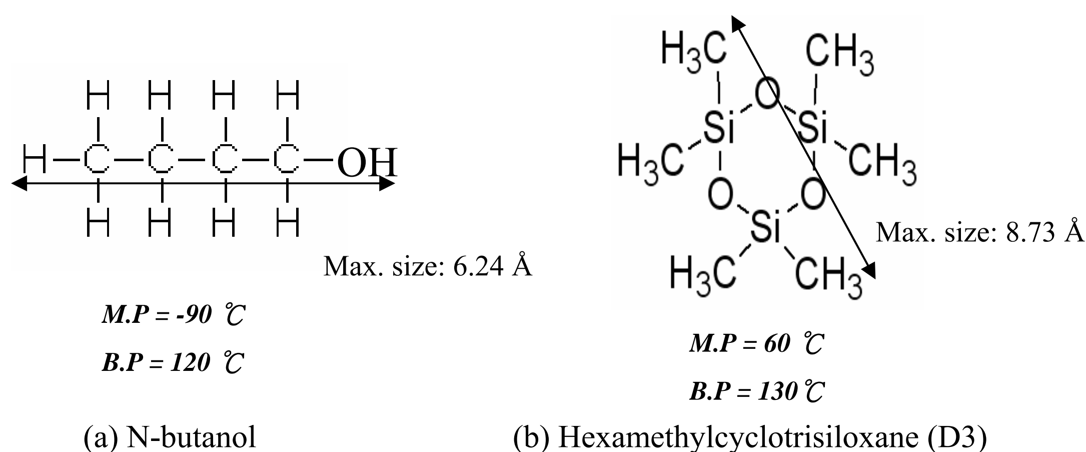

Figure 4.3 Structures of (a) N-butanol and (b) D3

4.2 Characterization of Pore-Sealing Treatment

4.2.1 Pore-Sealing Treatment by N-Butanol

First, N-butanol was utilized to seal the pores of porous silica before the mixture of low-k underfill material E. Unfortunately, the low-k underfill material E, after curing reaction, exhibited three serious problems; namely: (1) bad mechanical strength, (2) bubbles on the surface, and (3) phase separation, as shown in Figures 4.4 (a) through (c), which were discussed briefly below.

(a) Bad mechanical strength

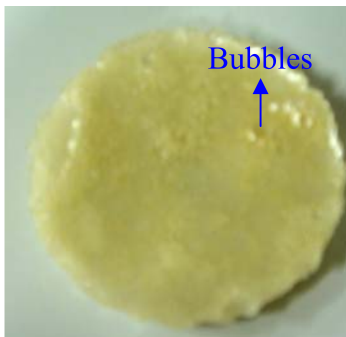

(b) Bubbles on the surface

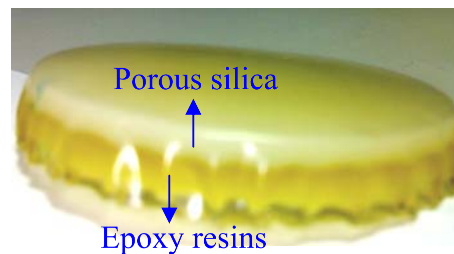

(c) Phase separation

Figure 4.4 Three issues of cured low-k underfill material E: (a) bad mechanical strength, (b) bubbles on the surface and (c) phase separation

(1) Bad mechanical strength:

Figure 4.5 showed the DSC curve of low-k underfill material E. By the comparison of DSC curves between low-k underfill material B and low-k underfill material E, it was found that the onset temperature of curing reaction was advanced from 125 ℃ (low-k underfill material B) to 110 ℃ (low-k underfill material E). In order to check if the curing reaction originated from epoxy resins and N-butanol further, we prepared another formulation marked “A” as shown in Table 4.1. Figure 4.6 was the DSC curve of formulation underfill material A which displayed that the curing temperature was from 110 ℃ to 135 ℃. Based on the DSC curves, we confirmed that epoxy resins reacted with N-butanol at the temperature from 110 ℃ to 135 ℃. Unfortunately, N-butanol had only one functional group. Therefore, the curing reaction between epoxy resins and N-butanol resulted in lower crosslink density than pure epoxy resin. The terrible mechanical strength was attributed to the lower crosslink density.

(2) Bubbles on the surface

From the DSC curve of formulation underfill material A, we discovered a peak at 175 ℃. It meant the residual N-butanol was trapped by the cured epoxy resins. Until 175 ℃, N-butanol evaporated at the moment and formed the bubbles on the surface.

(3) Phase separation of the porous silica and epoxy resins

With the addition of N-butanol, low-k underfill material E possessed very low viscosity. In this state, phase separation was easy to occur due to the different densities of epoxy resins and porous silica fillers.

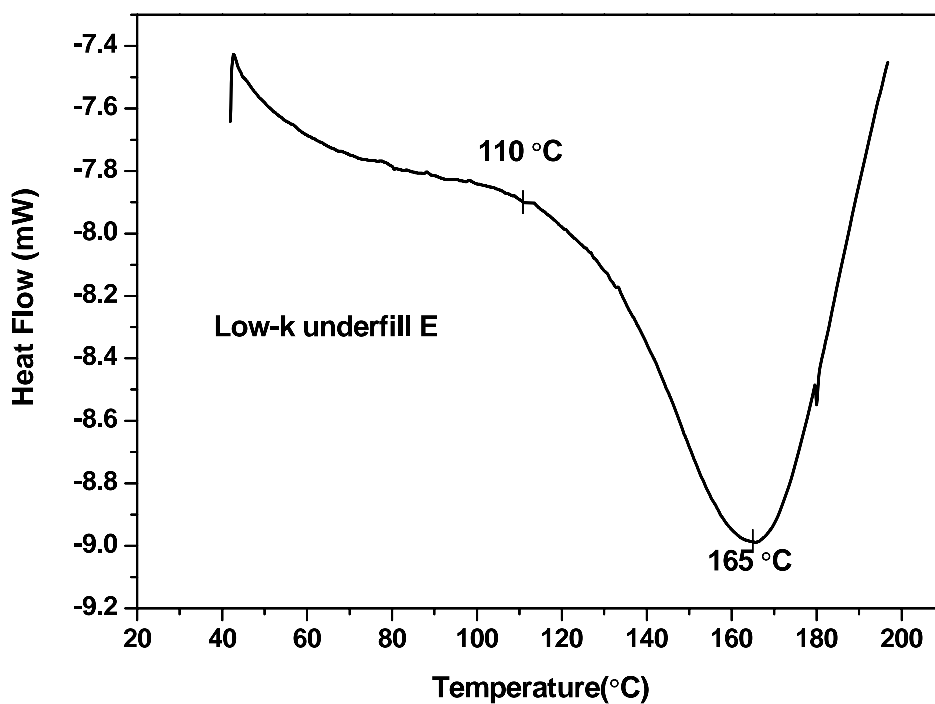

Figure 4.5 DSC curve of low-k underfill material E

Table 4.1 Formulation underfill material A

	Formulation underfill material A
Organic part (85 wt %)	Epikote828 Epikote862 2E4MI
Filler (15 wt %)	Porous silica with pretreatment
Pore-sealing Material	N-butanol

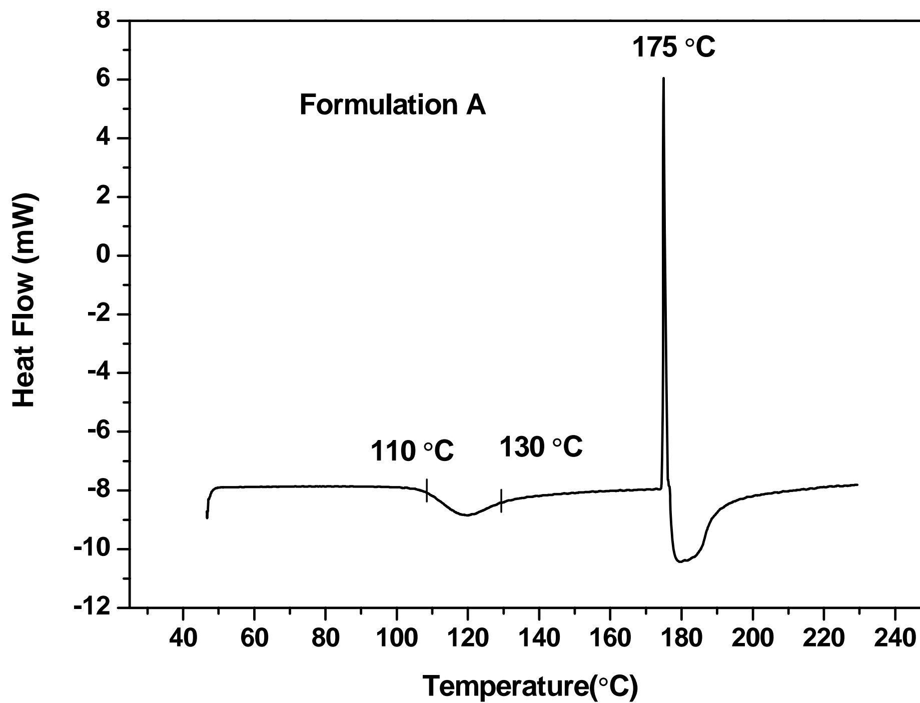

Figure 4.6 DSC curve of Formulation underfill material A

N-butanol possessed proper boiling point to serve as pore-sealing materials. However, it reacted with epoxy resins resulting in terribly poor mechanical strength due to these problems, N-butanol was not an appropriate material to carry out the pore-sealing pretreatments.

According to the pore-sealing pretreatment by N-butanol, besides the boiling point, compatibility, and molecular size, the other consideration for choosing pore-sealing materials was its reactivity. Pore-sealing materials cannot react with epoxy resins which may degrade the mechanical strength.

4.2.2 Pore-Sealing Treatment by Hexamethylcyclotrisiloxane (D3)

Figure 4.7 illustrated the DSC curve of low-k underfill materials with pore-sealing treatment by D3. In Figure 4.7, it showed two observations:

(1) There was an endothermic reaction occurring at about 60℃, which could be attributed to the melting of D3.

(2) The curing reaction started at 125℃ and completed at 190℃.

Compared to Figure 4.1 (DSC curve of low-k underfill material B), the curing reactions of these two curves were nearly the same at 125 ~ 190℃ which proved that D3 did not react with epoxy resins unlike N-butanol.

D3, with the boiling point at 130℃, could serve as a sacrificial material to carry out the pore-sealing treatment for porous silica fillers. D3 was mixed with porous silica fillers at desired weight ratio (porous silica/D3) of 1:1 and 1:3 in low-k underfill material C and low-k underfill material D, respectively. In the later sections, the morphology of D3/porous silica and pore sealing mechanism were studied by SEM and Brunauer-Emmett-Teller (BET) gas absorption method.

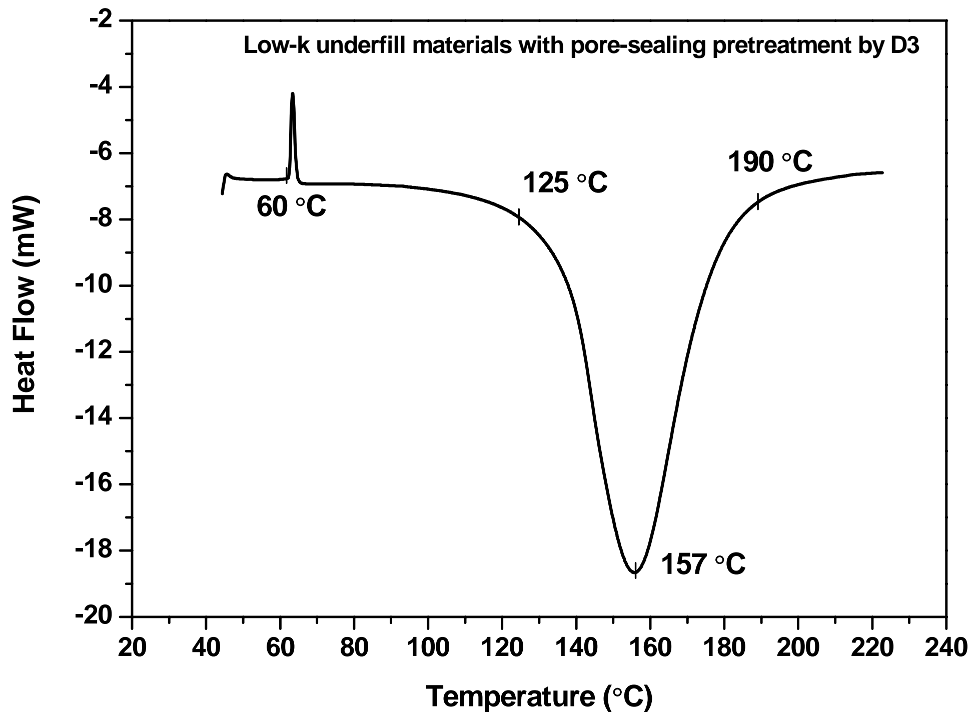

Figure 4.7 DSC curve of Low-k underfill materials with pore-sealing pretreatment by D3

4.2.2.1 Morphology of D3 materials and porous silica fillers

Scanning electron microscopy (SEM) was utilized to investigate the morphology of porous silica fillers with and without pore-sealing pretreatments. Figures 4.8(a) and 4.8(b) showed the morphology of D3 and pure porous silica, respectively. D3 had smooth surface while the porous silica was very rough. It was very easy to distinguish D3 from porous silica. From Figure 4.8(b), pure porous silica had a sponge-like structure which was presumably composed of large number of pores randomly dispersed and interconnected in silica matrix. The porous structure enabled the porous silica to have high absorbability. Figure 4.8(b) also indicated that the pores were in the nanometer scale while the size of D3 was in the angstrom scale which D3 could be absorbed by porous silica to seal the pores.

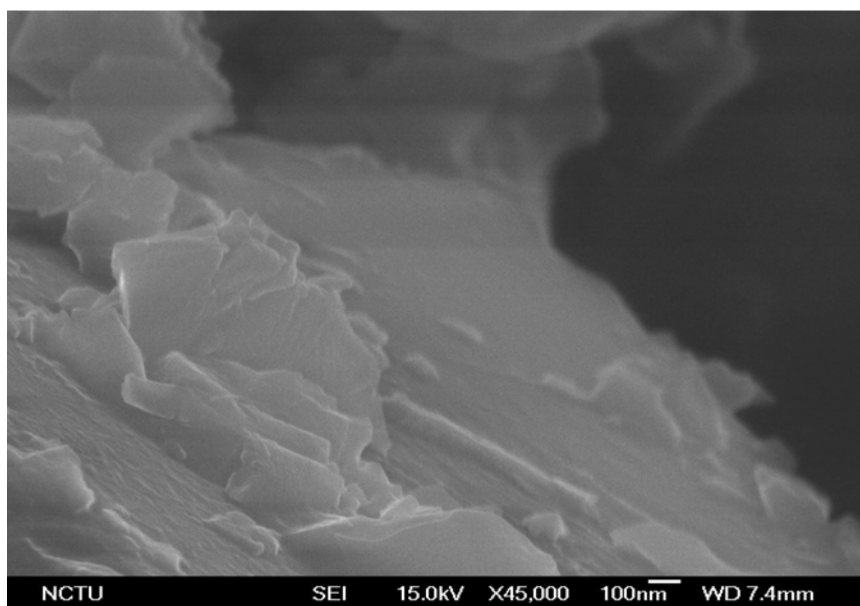

(a) hexamethylcyclotrisiloxane (D3)

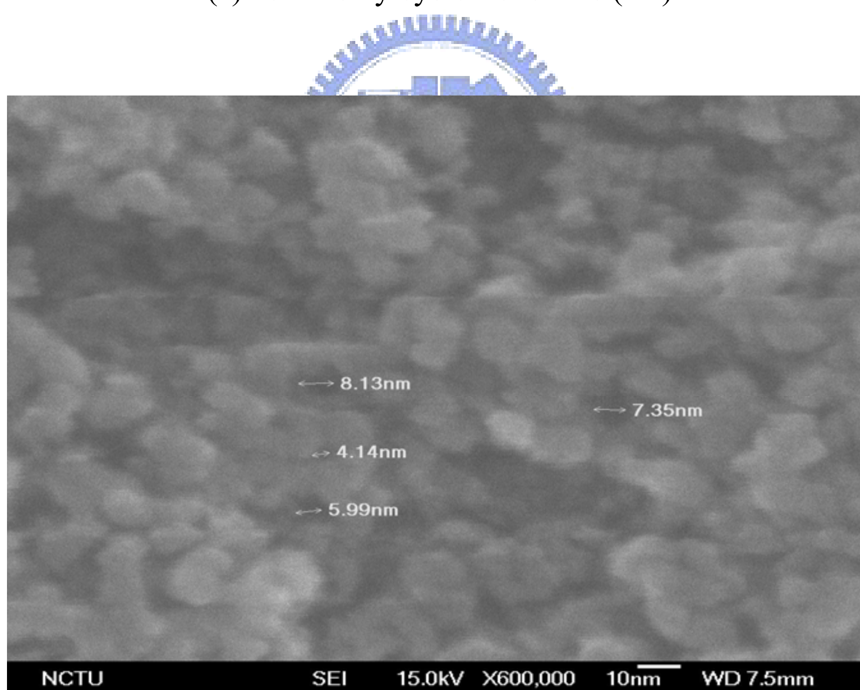

(b) Porous silica

Figure 4.8 Morphology of (a) hexamethylcyclotrisiloxane (D3) and (b) porous silica by SEM

Next, Figures 4.9(a) and 4.9(b) illustrated the SEM morphology of porous silica after pore-sealing treatments at 1:1 and 1:3 weight ratio (porous silica/D3) for low-k underfill material C and low-k underfill material D, respectively.

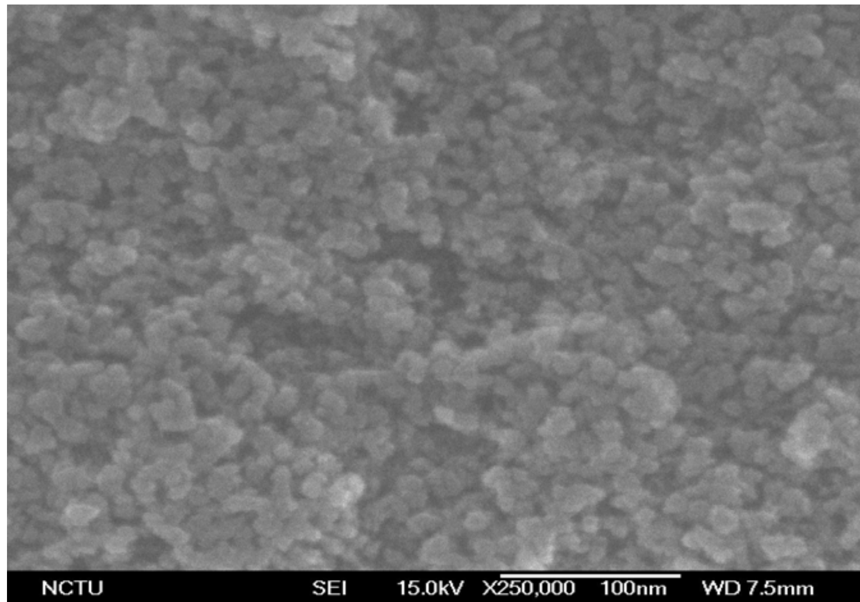

(a) Porous silica in low-k underfill material C (1:1)

(b) Porous silica in low-k underfill material D (1:3)

Figure 4.9 Morphology of porous silica after pore-sealing treatment in (a) low-k underfill material C and (b) Low-k underfill material D by SEM

For porous silica with the 1:1 weight ratio (porous silica/D3) pore-sealing pretreatment, it was hard to find D3 on the silica surface, indicating that D3 was well absorbed by pores into the inner of porous silica fillers. As more D3 was added to its mixture with porous silica (low-k underfill material D), D3 overflowed onto outer surface and left a uniform coating outside the porous silica fillers as illustrated in Figure 4.9(b). It appeared that during pore-sealing treatment at 95℃, D3 in liquid phase was absorbed into the inner pores of porous silica particles. With more and more amount added, the sacrificial materials, D3, overflowed onto outer surface.

4.2.2.2 Brunauer-Emmett-Teller Method (BET)

Subsequently, Brunauer-Emmett-Teller (BET) gas absorption method was used to measure pore volume, specific surface area, porosity and pore size distribution of underfill systems with and without pore-sealing pretreatment. Since the conventional solid silica filler exhibited extremely low level of porosity, BET measurement and analysis were primarily applied to the porous silica in low-k underfill materials B, C, and D as shown in Figures 4.10, 4.11, and 4.12, respectively. The shape of the BET curves indicated the pore size of porous silica was typically mesoporous type which meant that the pores ranging from 2 nm to 50 nm. In addition, in different underfill systems, the absorption volumes of porous silica in decreasing order was pure porous silica > low-k underfill material C > low-k underfill material D. It showed the infusion of D3 increased with the increasing D3/porous silica weight ratios.

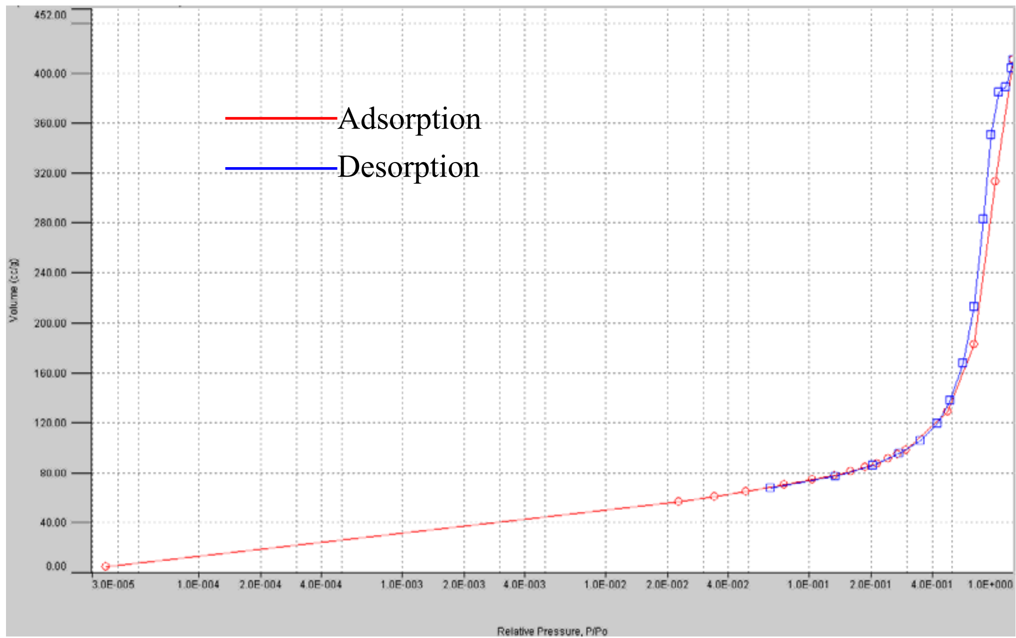

Figure 4.10 BET curve of low-k underfill material B

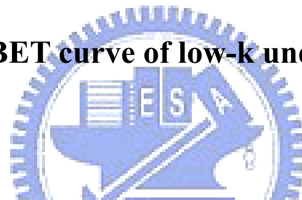

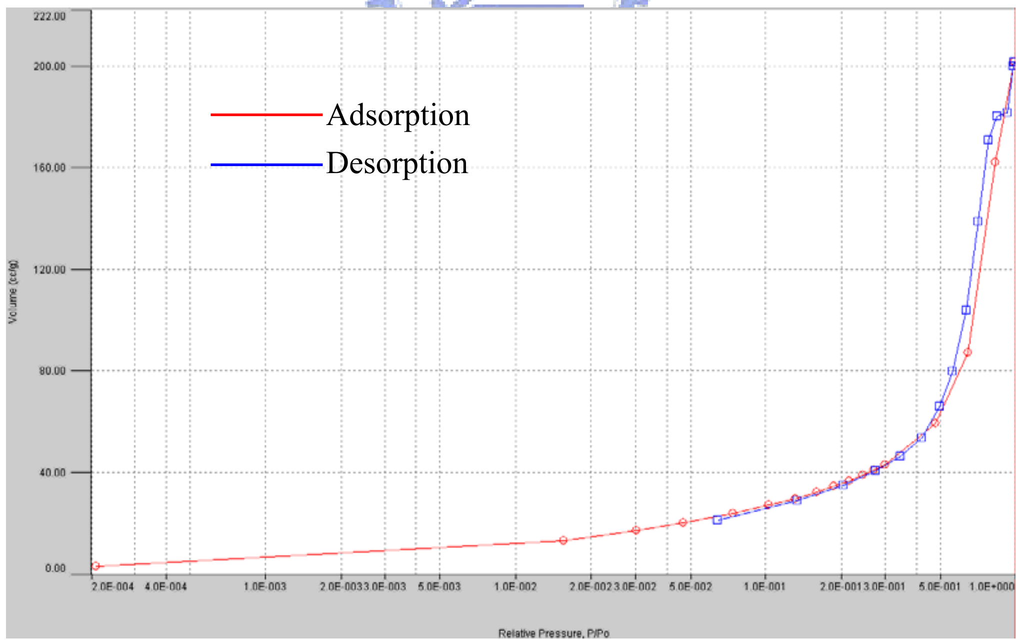

Figure 4.11 BET curve of low-k underfill material C

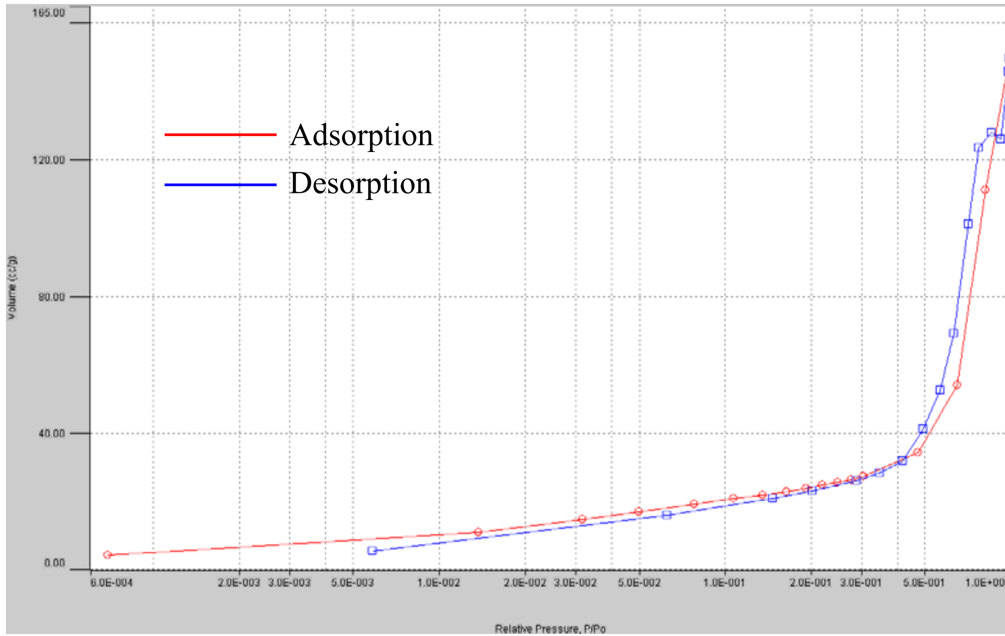

Figure 4.12 BET curve of low-k underfill material D

Table 4.2 summarized the pore volume, specific surface area, and porosity of porous silica in low-k underfill materials B, C, and D. Pure porous silica possessed 306 m^2/g surface area and 0.64cm^3/g pore volume with 60% porosity, which were relatively high to provide high absorbability. However, the surface area and pore volume of porous silica in low-k underfill material C were reduced to 53% and 52% of original value in pure porous silica after infusion of D3 at 1:1 ratio. When D3 concentration was increased to 3:1 D3/porous silica weight ratio, the surface area and pore volume of porous silica were further reduced to 72% and 64% of pure porous silica, respectively. In addition, it was found that the decreasing rate of surface area was larger than pore volume from Table 4.2. It implied that D3 could seal small-size pores more easily than big ones. Therefore, even infusion and adsorption of D3 was readily easy by its low viscosity, slight and preferential outgassing in the larger pores may result in completely sealed pores in smaller pore size, and left a D3 coating layer on the sidewall of larger pores due to surface tension. . When porous silica was treated with oversaturated D3, more retained pore volume was achieved under enhanced

concentration gradient. A decrease of mixing temperature may further enhance the retention of the amount of D3 within the interconnected structure

Table 4.2 BET data of porous silica in low-k underfill materials B, C, and D

	Low-k Underfill material B Pure Porous silica	Low-k Underfill material C Porous silica with pretreatment (1:1 weight ratio of silica/D3)	Low-k Underfill material D Porous silica with pretreatment (1:3 weight ratio silica/D3)
Surface area (m^2/g)	306	143	85
Pore volume (cm^3/g)	0.64	0.31	0.23
Porosity (%)	60	40	33

Next, Figures 4.13-4.15 showed the pore size distribution of porous silica with three different pretreatments in low-k underfill materials B, C, and D, respectively. Figure 4.16 summarized the pore size distribution curves of these three systems for comparison. For the pure porous silica without pore-sealing pretreatment in low-k underfill material B, pore size ranged up to ~150 nm with an average size of 6.6 nm. For porous silica with different pore-sealing pretreatment, 1:1 weight ratio of porous silica to D3 in low-k underfill material C and low-k 1:3 weight ratio of porous silica to D3 in low-k underfill material D, the average pore size was reduced from 6.6 nm to 5.3 nm due to pore filling, while pore size distribution curves of porous silica in low-k underfill materials C and D were shifted down, showing that the volume fraction of larger pores are also significantly reduced.

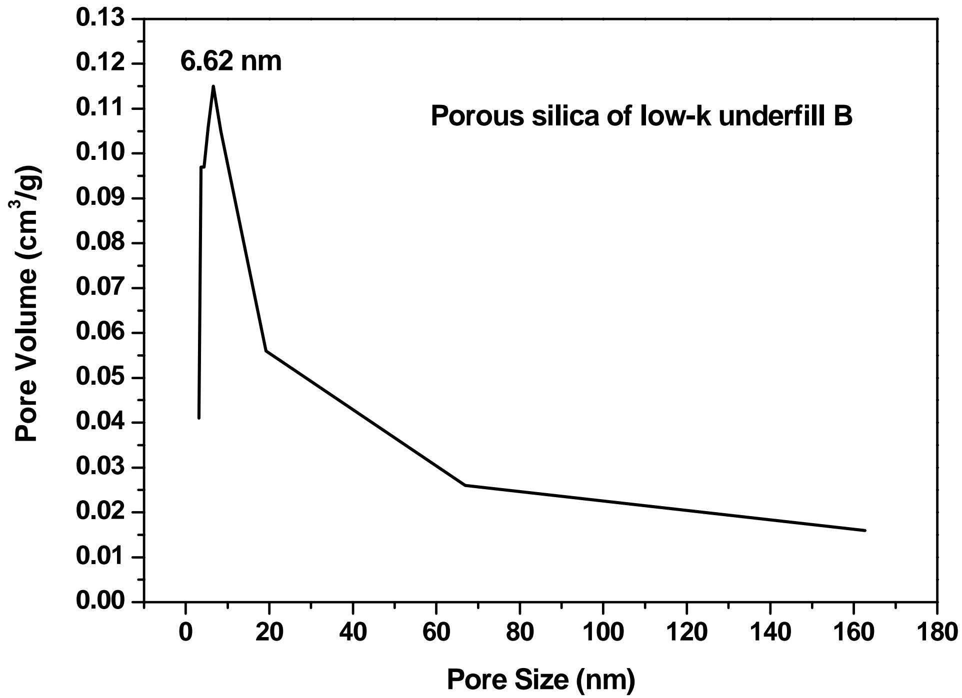

Figure 4.13 Pore size distribution of porous silica in low-k underfill material B, without pore-sealing pretreatment

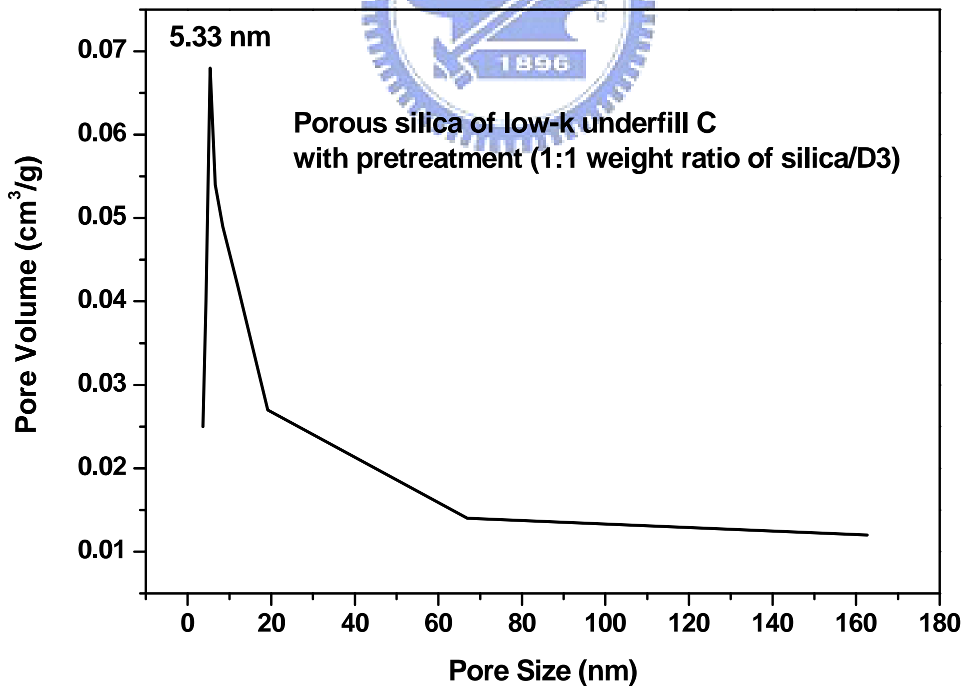

Figure 4.14 Pore size distribution of porous silica in low-k underfill material C, with pore-sealing pretreatment at 1 : 1 weight ratio

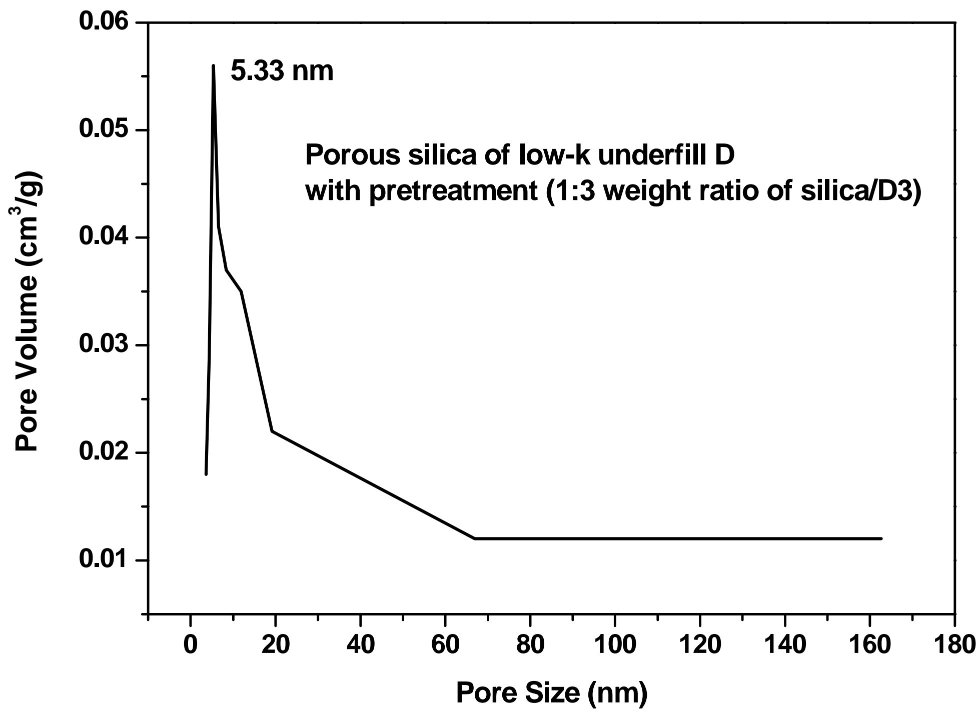

Figure 4.15 Pore size distribution of porous silica in low-k underfill material D, with pore-sealing pretreatment at 1 : 3 weight ratio

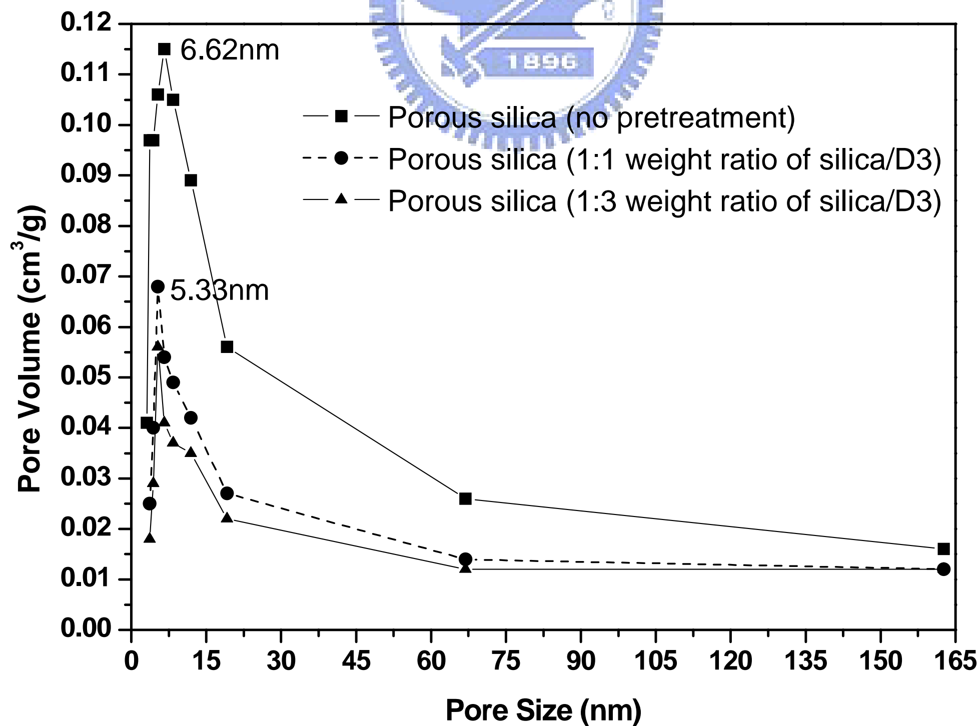

Figure 4.16 Comparison of these pore size distributions of porous silica with three different pretreatments

Equation (4.1) [19] was employed to predict the time required to fill a gap by capillary force. During the pore-sealing pretreatment by D3, the viscosity and surface tension of D3 were 0.001Pa · Sec and 0.024N/m; the average pore size of pores in porous silica was 6nm. The contact angle of D3 onto porous silica was assumed to be about 0° because inorganic D3 material was compatible with silica. From Equation (4.1), the time required to fill the pores was 0.0004sec which liquid D3 could fill the pores easily during pore-sealing pretreatment at 95℃.

$$t_{fill} = \frac{6\eta L^2}{\sigma h Cos\theta} \tag{4.1}$$

where:

t_{fill}: reguired time

η : viscosity

L: length

σ : surface tension

θ : contact angle

Based on the predicted time from Equation (4.1), BET data, and SEM images, we considered the pore-sealing pretreatmenmt involved the following two steps:

1st step: During the pore-sealing pretreatment at 95℃, liquid D3 easily and quickly filled the pores.

2nd step: Upon completion of pretreatment and mixing at 95℃, D3 would outgas to the ambient while the porous silica/D3 mixture was cooled down to room. There were two scenarios in this step: (1) For pore sizes below a threshold dimension, the small pores trapped the D3 without loss and (2) For pore sizes above the critical dimension,

partial D3 would loss from the large pores, leaving a D3 coating layer on the sidewall.

A simple two-step model of pore-sealing pretreatment by D3 was proposed and schematically illustrated in Figure 4.17 by ignoring the interconnectivity among pores through channels for simplicity.

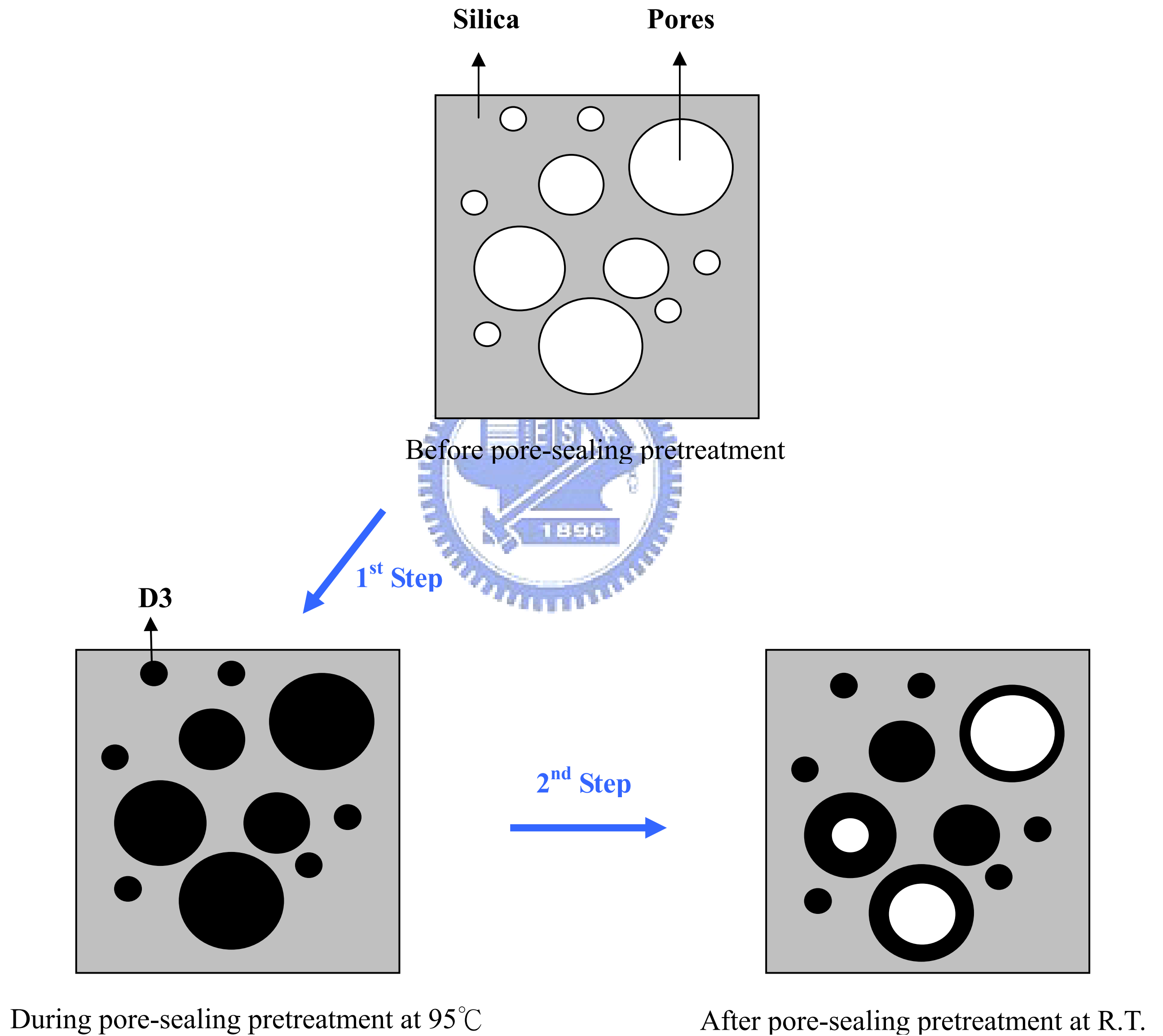

Figure 4.17 2-D pore-sealing model

4.3 Dielectric constants of low-k underfill materials

The dielectric constants of various cured underfill materials, measured by RF impedance-material analyzer at 1 GHz frequency, were summarized in Table 4.3.

Table 4.3 Dielectric constants of various underfill materials

	Dielectric constant (1 GHz)
Conventional capillary underfill	3.20
Low-K underfill material A	3.07
Low-K underfill material B	3.20
Low-K underfill material C	2.96
Low-K underfill material D	2.86

The low-k underfill material B had the same dielectric constant with conventional capillary underfill. This indicated that the pores in the porous silica of low-k underfill material B were all back-filled with epoxy resins without retained pores and thus showed no reduction in the dielectric constant. In contrast, underfill materials such as low-k underfill materials C and D with pretreatments for porous silica showed the reductions of the dielectric constants, 7.5% and 10.6%, respectively, which could be attributed to the retained pores from pore-sealing pretreatment. Next, we utilized Equation (4.2) [45] to predict the dielectric constants of composite materials and compare with the experimental data.

$$LogK = \sum Vi \cdot LogKi \tag{4.2}$$

where

K: the dielectric constant of composite materials

Vi: the volume fraction of i-th component

Ki: the dielectric constant of i-th component

The retained pore volume after curing reaction was assumed to be equal to the pore volume sealed by D3 pore-sealing pretreatment. By using Equation (4.1), the predicted dielectric constants of low-k underfill materials C and D were 2.9 and 2.8, respectively. Compared to the measured dielectric constants, 2.96 and 2.86, the discrepancy was within 3%. The result indicated that the validity of our assumption. Also, the pore-sealing pretreatment for low-k underfill materials C and D indeed delivered the expected effect in retaining the porosity and thus reduced the dielectric constants. The pore-sealing pretreatment by D3 successfully retained pore volume to reduce dielectric constants in two steps:

(1) Before curing reaction:

Pore sizes below a threshold dimension (< 15-20 nm) were sealed by D3 material, and therefore raw epoxy resins could not enter the pores at room temperature

(3) During curing reaction:

D3 boiled at 120 ~ 140℃ during curing reaction, which outgassed out of the pores and hindered the backfill of epoxy resins into the pores with a positive, outward pressure until the completion of curing reaction.

As previously mentioned, low-k underfill material A was taken as the control group compared to low-k underfill materials B, C, and D. Zeeospheres, as the fillers in low-k underfill material A, had the different type of pores from the porous silica in low-k underfill materials B, C, and D . Zeeospheres were silica-alumina balls whose structure was illustrated schematically in Figure 4.18 [46]. From Table 4.3, low-k underfill material B had higher dielectric constant (3.2), which was even higher than

low-k underfill material A (3.07) due to non-retained pores after curing reaction. Zeeospheres offered another type of pores to reduce dielectric constants. This will be a separate study in the future.

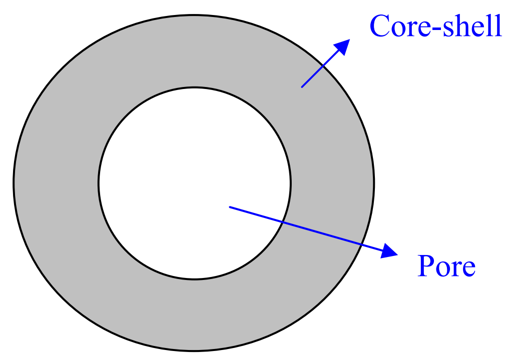

Figure 4.18 Structure of zeeospheres

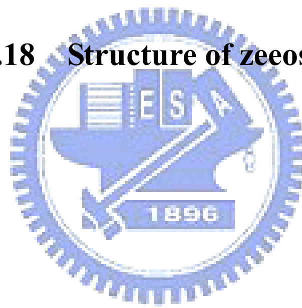

4.4 Moduli of low-k underfill materials

In this section, DMA was employed to characterize the mechanical strength of different underfill materials as summarized in Table 4.4.

Table 4.4 Moduli of various underfill materials

	Modulus (at 40 ℃)	Filler
Conventional capillary underfill	3.0	solid silica
Low-k underfill material A	2.4	Zeeospheres
Low-k underfill material B	2.6	porous silica
Low-k underfill material C	1.5	porous silica
Low-k underfill material D	1.8	porous silica

These underfill materials could be classified into three groups by the different types of fillers.

(1) Solid silica

(2) Zeeopheres

(3) Porous silica

It was found that the moduli of various underfill materials in decreasing order were: underfill with solid silica (conventional capillary underfill) > underfill with porous silica (low-K underfill material B) > underfill with zeeospheres (low-k underfill material A). Undoubtedly, conventional capillary underfill at the same silica content had the highest modulus because of its dense structure without any pores in the matrix. Noticeably, although low-k underfill material B had no retained pore volume like conventional capillary underfill due to the backfill of epoxy resins into pores, the modulus of low-k underfill material B was lower. Such low mechanical strength could

be attributed to weaker strength of porous silica and possibly poor adhesion at epoxy resin/porous silica interface.

Furthermore, the moduli of low-k underfill materials B, C, and D were characterized to examine any effect of pore-sealing pretreatment on the mechanical strength. From Table 4.4, the modulus of low-k underfill material B without pretreatment dropped 13.3% to 2.6 GPa. The moduli of low-k underfill materials C and D dropped 50% and 36.7%, respectively because of the open pores retained by the pore-sealing pretreatment. Further analysis was carried out by using Equation (4.3) to estimate the modulus of composite materials [47].

$$\frac{1}{E} = \sum \frac{Vi}{Ei} \tag{4.3}$$

where

E: ideal modulus of composite materials

Ei: modulus of i-th component

Vi: volume fraction of i-th component

Figure 4.19 showed the predicted moduls values according to Equation (4.3) and experimental data of low-k underfill materials B, C, and D.

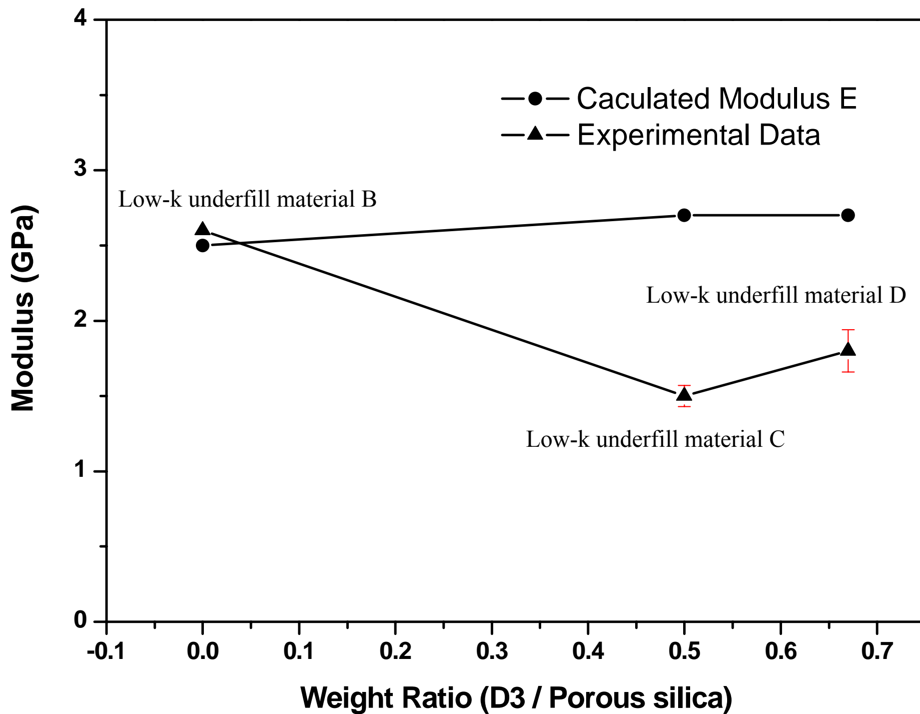

Figure 4.19 Moduli of calculated values and experimental data of low-k underfill materials B, C, and D

In Figure 4.19, the modulus of low-k underfill material B was nearly equal to the calculated value; however, the moduli of low-k underfill materials C and D were obviously lower than E. According to Equations (3.12) and (3.13) in Section 3.3.5.2, it indicated that, in the same two-component system, higher tanδ resulted from more energy dissipation due to poor adhesion between these components [44]. Therefore, the moduli of low-k underfill materials C and D, lower than E obviously, may be attributed to the poor interface between epoxy resins and porous silica. This hypothesis was further confirmed by the loss factor obtained from DMA measurement, tanδ, of various low-k underfill materials as summarized in Table 4.5. A high Tanδ indicated that high internal energy dissipation due to poor adhesion. Therefore, as the ratio of D3/porous silica increased, Tanδ(s) values of low-k underfill materials B, C,

and D increased from 0.02 to 0.06, representing that the adhesion of epoxy and porous silica became weaker resulting in degradation of moduli in the underfill composite.

Table 4.5 Loss factor, tan δ of low-k underfill materials B, C, and D

	Tanδ (at 40 ℃)
Low-k underfill material B	0.02
Low-k underfill material C	0.04
Low-k underfill material D	0.06

To search for physical evidence of poor adhesion between epoxy resins and porous silica, SEM was employed to investigate the morphology of the cross-section of cured underfill materials. Figure 4.20 showed the cured underfill materials without pore-sealing pretreatment (low-k underfill material B) while Figure 4.21 illustrated the cured underfill materials (low-k underfill materials C and D) which went through the pore-sealing pretreatment. By comparison of the morphology in Figures 4.20 and 4.7 (b), the cured low-k underfill material B had rough surface which was similar with the surface of porous silica. It was believed that the pores in the silica of low-k underfill material B, without pore-sealing pretreatment, were all back-filled with epoxy resins so that epoxy resins overflowed onto outer surface and left a coating outside the porous silica particles. In contrast, delamination was found at the interface between the epoxy resins and porous silica. Combining Tanδ in Table 4.5 and SEM images in Figure 4.21, we proved that, during the crosslinking reaction of low-k underfill materials C and D, D3 vaporized out of pores and destroyed the adhesion of epoxy resins and fillers. As a result, the pore-sealing pretreatment indeed degraded the

mechanical strength.

It is imperative to enhance the adhesion at epoxy/porous silica interfaces when pretreatment by mixing sacrificial materials and porous silica is considered. The options included: (1) addition of adhesion promoter(s) in the formulation, or (2) a sacrificial material possessed a lower vapor pressure at crosslinking temperature, or (3) xxx, which are the topics for future work.

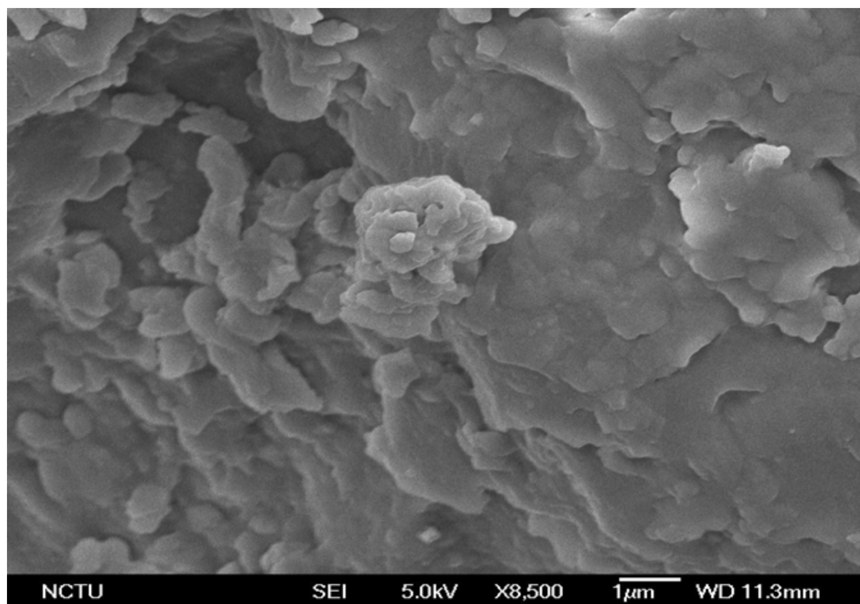

Figure 4.20 Morphology of cured underfill materials without pore-sealing pretreatment (low-k underfill material B) by SEM

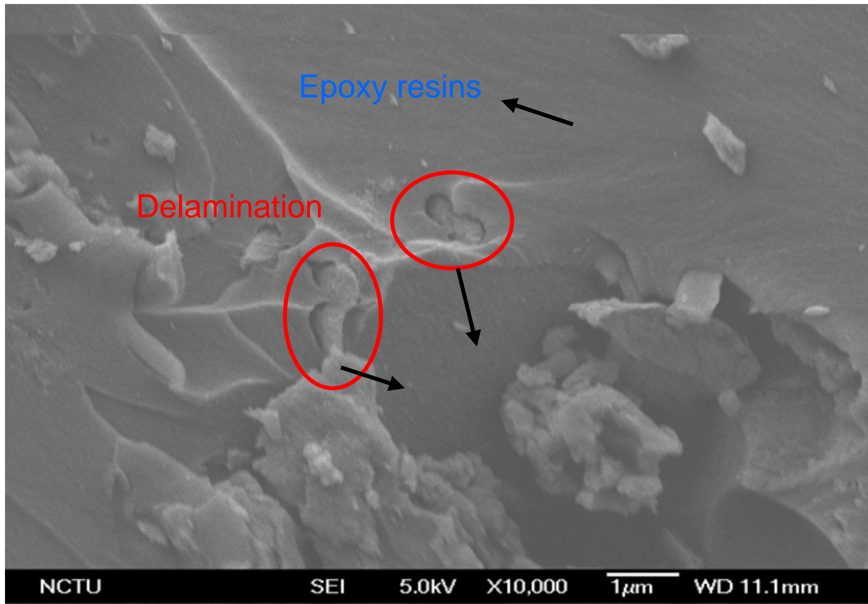
Epoxy resins
Delamination
NCTU SEI 5.0kV X10,000 1μm WD 11.1mm

E S A
1896

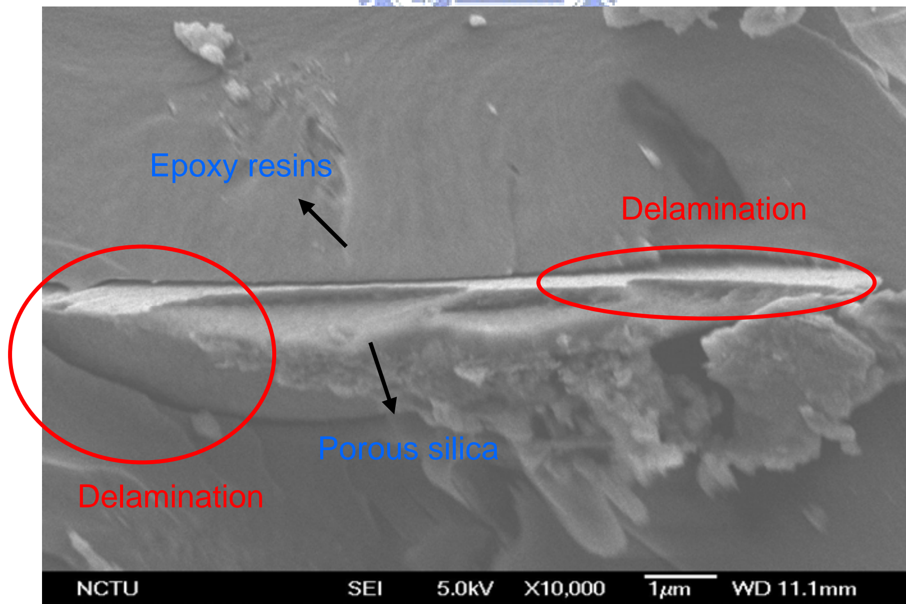
Epoxy resins
Delamination
Porous silica
Delamination
NCTU SEI 5.0kV X10,000 1μm WD 11.1mm

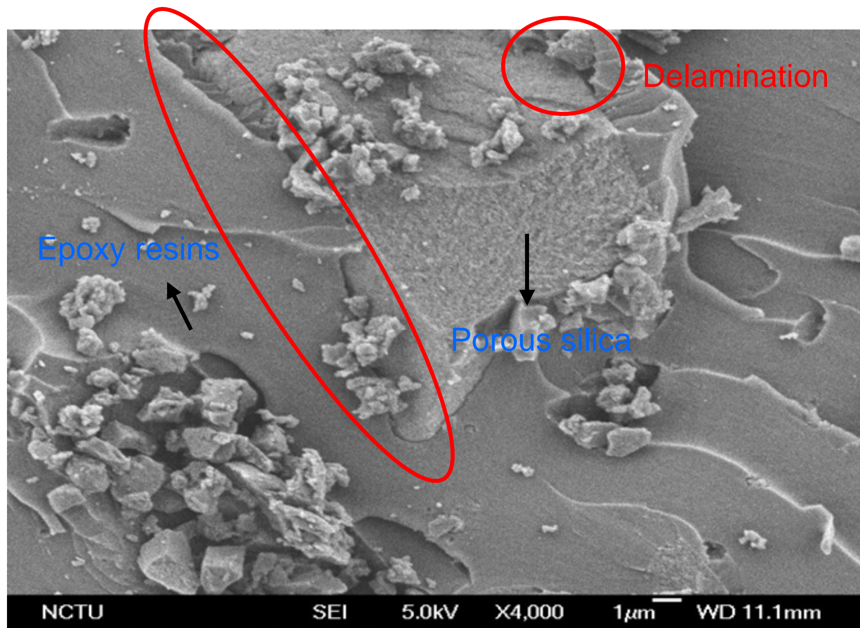

Figure 4.21 Morphology of cured underfill materials with the pore-sealing pretreatment (low-k underfill materials C and D) by SEM

Chapter 5 Conclusions

For RF devices applications, underfill materials shall possess low dielectric constants to improve RC delay, power consumption, and crosstalk noise, besides excellent mechanical strength. By the utilization of zeeospheres and porous silica as the fillers, porosity was successfully introduced into the underfill materials by pore sealing pretreatment to reduce their dielectric constants.

For the pore-sealing treatment of low-k underfill materials, the selection of an appropriate material to seal the pores was the most critical. The temperature-dependent viscosity and the curing reaction were found to be important in the selection of sacrificial material, while the curing profile for pore-sealing pretreatment could be determined by DSC and rheometer measurements. The material, employed for pore-sealing treatment, shall possess the properties described below:

(1) The material must have proper melting point such that it could sealed the interconnected pores, and appropriate boiling point to ensure that it could be removed thermally during the curing reaction of underfill materials.

(2) The materials should possess poor compatibility with epoxy resins which can hinder the epoxy resins to flow into the pores.

(3) The molecular size of the material must be smaller than the pore size of porous silica so that it can enter the pores easily to seal the pores.

(4) The material cannot react with epoxy resins degrading the mechanical strength of underfill materials.

In this thesis, a pore-sealing pretreatment for porous silica was developed by employing D3, with melting point, 60 ~ 70 ℃, and boiling point, 130 ~ 140 ℃. The

molecular size of D3 was below 1nm, which was far smaller than the pore size of porous silica (6.6nm), indicating that D3 could easily get into the pores to seal them. Moreover, it was good that D3 didn't react with the epoxy resins unlike N-butanol. These properties made D3 to protect and retain the porosity successfully. The mechanisms for retaining porosity in the underfill system could be illustrated in two stages; namely.

(1) The sacrificial material, D3, heated at 95 ℃, easily flowed into the pores and sealed over the pores such that the flowing epoxy resins could not enter the pores at room temperature. Upon the cooling step after pre-treatment, D3 trapped in the larger pores would slightly outgas leaving a layer of D3 onto the sidewall of pores. Some degree of epoxy backflow into larger pore was likely.

(2) D3 outgassed at boiling point, 120 ~ 140 ℃, at which large gas pressure out of pores hindered the reflow of the epoxy resins during the curing reaction until the high viscosity of epoxy resins resulting from crosslinking.

The pore-sealing pretreatment by D3 had successfully retained pores to reduce the dielectric constants of underfill materials such as low-k underfill materials C and D. However, D3 also led to 30-40% degradation of mechanical strength due to the poor adhesion at epoxy/porous silica interface caused by D3 outgassing. The hypothesis was further confirmed by loss factor, tanδ using DMA, which was an indicator to estimate the interface condition of composite materials. The higher tanδ meant more energy dissipated and poor adhesion between the components. For low-k underfill materials B, C, and D, tanδ data of low-k underfill material C and D (0.04 and 0.06) were larger than that of low-k underfill material B (0.02) which indicated that D3 vaporized and diffused out of pores during curing reaction, and therefore, destroyed the adhesion between epoxy and fillers.

In summary, we have successfully developed a pore-sealing pretreatment for porous silica fillers by D3 to reduce dielectric constant from 3.2 to 2.86 (~10.6%) with 15 wt% porous fillers in this thesis. However, the mechanical strength was reduced from 3.0 GPa to 1.5 GPa. because of poor adhesion at porous silica/epoxy interfaces caused by D3 ougassing during the curing reaction step.

References

[1] D. J. Frank, R. Puri, and D. Toma, Proceedings of the 2006 IEEE/ACM international conference on Computer-aided design, 329 (2006).

[2] L. T. Manzione, Plastic Packaging of Microelectronic Devices (Van Nostrand Reinhold, New York 1990).

[3] J. H. Lau, Flip Chip Technologies (McGraw-Hill, New York 1996).

[4] 黃淑禎，李巡天，陳凱琪，新世代半導體封裝材料與發展趨勢，工業材料 170，86 (2001).

[5] 郭嘉龍，半導體封裝工程 (全華科技圖書公司，台北市 1999).

[6] S. Luo, Tsuyoshi Yamashita, and C. P. Wong, Adhesive Joining and Coating Technology in Electronics Manufacturing, 70 (2000).

[7] 楊正杰，張鼎張，鄭晃忠，銅金屬與低介電常數材料與製程，毫微米通訊 7，40 (2000).

[8] D. R. Frear, Future Fab Intl. **16,** 10 (2004).

[9] R. Kultzow and B. Mainguy, Electrical Insulation Conference and Electrical Manufacturing and Coil Winding Conference, 291 (2001)

[10] R. R. Tummala, Fundamentals of Microsystems Packaging (McGraw-Hill, New York 2001).

[11] 呂宗興，電子構裝技術的發展歷程，工業材料 115，49 (1996).

[12] J. H. Lau, Ball Grid Array Technology (McGraw-Hill, New York 1995).

[13] 鐘文仁，陳佑任，IC 封裝製程與 CAE 應用 (全華科技圖書公司，台北市 2005).

[14] Y. Liu, D. Desbiens, S. Irving, and T. Luk, IEEE Proc. of 55th ECTC, 861 (2005).

[15] 孔令臣, Flip Chip Bumping Technology, 工業材料 **139**, 155 (1998).

[16] C. P. Wong, S. Lou, and Z. Zhang, Science **290**, 2269 (2000).

[17] J. W. Nah, K. Chen, and K. N. Tu, J. Mater. Res **22**, 763 (2007).

[18] J. H. Lau, Low Cost Flip Chip Technologies (McGraw-Hill, New York 2000).

[19] Z. Zhang and C. P. Wong, IEEE T. Adv. Packaging **27**, 515 (2004).

[20] H. Lu, G. Glinski, and C. Bailey, APACK 2001 Conference on Advances in Packaging, 245 (2001).

[21] Y. San, Study on the Nancomposite Underfill for Flip-Chip Application, Georgia Institute of Technology (2006).

[22] 賴耿陽, 環氧樹脂應用實務 EPOXY RESINS (復漢, 台南市 1993).

[23] E.J.A Pope and J.D. Mackenzie, Journal of Non-Crystalline Solids **87**, 185 (1986).

[24] K.C. Chen, T. Tsuchiya, and J.D. Mackenzie, Journal of Non-Crystalline Solids **81**, 227 (1986).

[25] A. H. Boonstra and T. T. M. Bernards, Journal of Non-Crystalline Solids **105**, 207 (1988).

[26] D. Suryanarayana, R. Hsiao, T. P. Gall, and J. M, Mccreary, IEEE Transaction of Components and Hrbrid and Manufacturing Technology **16**, 858 (1993).

[27] K. M. Chen, D. S. Jiang, N. H. Kao, and J. Y. Lai, Microelectronics Reliability **46**, 155 (2006)

[28] P. S. Ho, J. Leu, and W. W. Lee, Low Dielectric Constant Materials for IC Applications (Springer, Berlin, 2003)

[29] P.-H. Tsao, C. Huang, M.-J. Lii, B. Su, and N.-S. Tsai, Electronic Components and Technology Conference, 767 (2004)

[30] C. George and T. Michael, IEEE/SEMI Int'l Electronics Manufacturing Technology Symposium, 10 (2004)

[31] H. Kusamitsu, Y. Morishita, K. Maruhashi, M. Ito, and K Ohata, IEEE T. Electron Pack. **22**, 23 (1999).

[32] S. P. Murarka, M. Eizenberg, and A.K. Shinha, Interlayer Dielectrics for Semiconductor Technologies (Elsevier, London 2003).

[33] J. Lou and W. Chen, IEEE Design and Test of Computers **21**, 24 (2004).

[34] Z. Tao, L. Fan, and S. Yang, 7th International Conference on Electronics Packaging Technology, 1 (2006)

[35] J. R. Lee, F. L. Jin, S. J. Park, and J. M. Park, Surface and Coatings Technology **180**, 650 (2004)

[36] International Technology Roadmap for Semiconductors (2003)

[37] I. Sugiura, N. Misawa, and Y. Nakata, Microelectronic Eng. **82**, 380 (2005)

[38] S. Li, Z. Li, and Y. Yan, Adv. Mater. **15**, 1528 (2003).

[39] Bershtein, Vladimir A., and Victor M., Differential Scanning Calorimetry of Polymers/Physics, Chemistry, Analysis, Technology (Ellis Horwood, New York, 1994)

[40] J. M. Dealy, Rheometers Molten Plastics: A Practical Guide to Testing and Property Measurement (Van Nostrand Reinhold Company, New York 1982)

[41] Y. L. Sun, A Room-Temperature Gas Sensor Based on Solid-State Lanthanum Fluoride Electrolyte, National Cheng Kung University (2002).

[42] N. Ku and K. Shi, RF Impedance/Material Analyzer (Hewlett Packard, Japan 1998)

[43] K. P. Menard. Dynamic Mechanical Analysis: A Practical Introduction (CRC Press, New York 1999)

[44] T. Murayama, Dynamic Mechanical Analysis of Polymeric Material (ELSEVIER, New York 1978)

[45] Y. Rao, J. Qu, T. Marinis, and C. P. Wang, IEEE T. Compon. Pack. **23**, 680 (2000)

[46] R. A. Caruso, A. Susha, and F. Caruso, Chem. Mater. **13**, 400 (2001)

[47] W. D William and J. Callister, Materials Science and Engineering: An Introduction (Wiley, New York, 2003)